Rehydroxylation (RHX) dating: Mass loss issues due to incomplete drying, carbon content, and mineral alteration

Barrett, G. (2017). Rehydroxylation (RHX) dating: Mass loss issues due to incomplete drying, carbon content, and mineral alteration. *Journal of Archaeological Science Reports*. https://doi.org/10.1016/j.jasrep.2017.02.001

Published in:
Journal of Archaeological Science Reports

Document Version:
Peer reviewed version

Queen's University Belfast - Research Portal:
Link to publication record in Queen's University Belfast Research Portal

Title:

Rehydroxylation (RHX) Dating: Mass Loss Issues due to Incomplete Drying, Carbon Content, and Mineral Alteration.

Author Name and Affiliation:

Gerard Thomas Barrett, Ph.D.

[14]CHRONO Center for Climate, the Environment, and Chronology, School of Natural and Built Environment, Queen's University Belfast, Elmwood Avenue, Belfast BT7 1NN, Northern Ireland, UK

Email: g.barrett@qub.ac.uk

Abstract:

As part of rehydroxylation (RHX) dating trials on post-medieval bricks, investigations were carried out into the presence, and effect on age estimations, of uncertainties associated with (a) prolonged and incomplete drying of samples, (b) the removal of organic and non-organic matter during heating, and (c) mineral alteration during heating. All samples exhibit an issue with a prolonged period of drying, exceeding two months at 130°C. Methods for treating this issue are applied and demonstrate the need for higher resolution and more precise monitoring of the mass loss during drying if the moisture not removed needs to be taken account of; this may not be necessary if prolonged drying is associated with the slow removal of chemisorbed water, distinct from rehydroxylation-related water loss. Organic matter contamination is also present in significant quantities in all samples, regardless of the retrieval context; the considerable effects of uncertainties in this quantity, arising from variability in the organic matter to organic carbon ratio (OM/OC), on age estimations are presented. Mineral alteration during reheating is generally negligible except when gypsum is present; large sources of uncertainty arising from moisture loss associated with dehydration and with subsequently lower levels of physisorption following reheating are highlighted as problematic.

Keywords:

Rehydroxylation, Dating, Drying, Contaminants, Minerals, Components

1. Introduction

The potential of rehydroxylation dating as an archaeological tool showed early promised (Wilson 2009; 2012) but has since suffered from an absence of successful applications (e.g. Burakov et al. 2013; Le Goff and Gallet 2015a; Numrich et al. 2015) and the identification of a range of issues surrounding the method (e.g. Bowen et al. 2011; 2013; Le Goff and Gallet 2015a; 2015b; Gallet and Le Goff 2015; see also the review in Barrett 2015). These often focus on the mass gain behavior that is central to the method, for example the suitability of a $t^{1/4}$ model (e.g. Bowen et al. 2011; Le Goff and Gallet 2014; 2015b; Gallet and Le Goff 2015; Barrett 2017b) or the equilibration of the mass following drying (e.g. Le Goff and Gallet 2014; Gallet and Le Goff 2015). However, there are also issues surrounding estimation of the amount of mass, due to rehydroxylation (uptake of atmospheric moisture that is subsequently chemically bound to the ceramic matrix), gained by the ceramic since it was last dehydroxylated (i.e. originally fired or last heated above 500°C). This mass is critical to age calculations and can be retrieved based on the mass loss that occurs during reheating at 500°C (Wilson 2012). There may be components of this mass loss that have other origins and need to be taken account of: incomplete drying (Bowen et al. 2011; Barrett 2015) may result in a quantity of loose or capillary water later removed at the higher reheating temperature; organic carbon may be burnt off between 200-500°C (Numrich et al. 2014); and minerals may undergo alteration and contribute additional mass loss, i.e. goethite (Burakov and Nachasova 2013). These mass loss issues, particularly incomplete drying and organic matter, have not received enough focused attention. As part of a larger work aimed at assessment of the archaeological application of RHX dating (Barrett 2015; 2017a; 2017b), these factors were explored, pre-planned in the case of organic contaminants and mineral alteration but necessitated unexpectedly in the case of indefinite drying; the dating trial results are presented in the companion article (Barrett 2017a).

The results of mass loss data for drying granulated samples will be presented together with modelling attempts to account for any remaining moisture (mass) in the fabric. The potential effect this estimated remaining mass has on age estimations from dating trials (Barrett 2015; 2017a) will be explored. As well as this, an explanation for prolonged drying will be suggested.

The presence and nature of organic matter, lost during heating, are examined using Fourier transform infrared spectroscopy (FTIR), carbon content analysis, and thermogravimetric mass spectrometry (TG-MS). The mass loss

uncertainties (and their age estimation impact) that arise from issues with the organic matter to organic carbon (OM/OC) ratio will be explored.

Finally, the effects of reheating on the mineral composition are examined through x-ray diffractometry (XRD) and FTIR.

Note that in the associated dating trials both mass gain models, $t^{1/4}$ and $t^{1/n}$, were applied for reasons discussed in Barrett (2017a). While the latter was preferred, the age estimations produced using both approaches were problematic. The present work discusses mass loss effects in relation to both, with preference often given to the use of the $t^{1/4}$ model results in illustrating the magnitude of potential effects (of relevance in re-examining successful RHX dating trials that used this model, i.e. Wilson et al. 2009; 2012); counterpart effects for the $t^{1/n}$ model can be found in Barrett (2015) and are not included here if the magnitude of the effect is very similar to that for the $t^{1/4}$ model such that it does not alter or contribute significantly to the main conclusions and arguments being made.

2. Method

2.1 Samples

The sample set (see supplementary materials *Table S1* and *S2*) is described in more detail (including compositional, surface area, firing information, origin, context) in the companion article (Barrett 2017a) and more comprehensively elsewhere (Barrett 2015). It was composed of 18 samples, including 14 brick samples from the island of Ireland, 2 pottery samples from Northern Ireland, and a piece of Roman and Etruscan ceramics; the brick and pottery samples were of post-medieval age (*Table S1*). Samples were retrieved from both buried (9) and non-buried (9) contexts (*Table S2*). Brick samples (of particular importance as they provided all 12 samples suitable for age estimates in Barrett 2015; 2017a) were likely produced from residual/boulder clays (rich in quartz and feldspars and generally low in calcium content) that were well fired above 850°C (Barrett 2015; 2017a). The specific surface area of samples was quite variable but typically < $5m^2/g$ (*Table S.3*).

2.2 Drying and Loose Water Modelling

Drying at 130°C was conducted during dating trials (Barrett 2015; 2017a) to remove any non-rehydroxyl moisture from the ceramic (i.e. pore or capillary bulk moisture). Samples had already undergone extensive pre-drying at approximately 80°C for 15 days during preparation before this stage (see Barrett 2015). For drying, granulated

samples (typically > 80g of 2-5.6mm sieved fractions, each granule approx.. 0.05-0.15g) were spread out on aluminium trays and placed in an oven (fan assisted) at 130°C (granulation was conducted to homogenize sample material, originally quite heterogeneous, before it was split into three subsamples for dating trials) . Based on the existing literature (see *Discussion*), it was assumed that samples would dry to constant mass within a reasonable period of time (maximum of a couple of weeks). On a near daily basis, the trays were removed and weighed on a top-loading balance under room conditions of 20 ± 1°C and 78 ± 3%RH. Samples were weighed under a rigid timing regime for two months; it was recognized from the mass loss curves that after a month of repeated measurements equilibration to constant mass appeared unlikely with measurements continued for an additional month to improve the quality of the mass loss curves.

Modelling of the drying curves was carried out to provide an estimate of the magnitude of loosely bound water, m_{lw}, not removed during drying (presumed to be removed when samples are reheated at 500°C as part of dating trials). Two empirical models of drying were applied using the curve fitting tool *cftool* in *MATLAB R2012a*:

Model 1 (Power): $m(t) = a(t^{-b})+c$ (a)

where a is the mass rate, b is the power of the model, and c is the final dry mass of the ceramic.

Model 2 (Exponential): $m(t) = ae^{-bt} + c$ (b)

where a and b (drying constant) are coefficients that determine the rate of moisture loss and c the final dry mass of the ceramic.

The former of these models was trialled based on the emphasis of the prevalence of $t^{1/2}$ transport processes in ceramic materials (Brosnan and Robinson 2003). However, it was found that the ½ power was a poor descriptor of the behaviour observed; hence the power constraint was relaxed.

The latter of these two models is derived from Lewis' (1921) thin-layer equation:

$$\frac{dX}{dt} = b(X - X_e) \quad \text{(c)}$$

where X is the moisture content, X_e is the equilibrium moisture content (i.e. 0 for an idealised dry ceramic) and b is the drying constant. Lewis (1921) considered that during drying of porous and hygroscopic materials, the rate of loss of moisture is proportional to the difference between the moisture content and the moisture content when the material

is at equilibrium (dry) with the drying environment. This *thin-layer* equation assumes that the conditions of drying (humidity, temperature) are constant throughout the material during drying. Forms of this equation are commonly used in fundamental modelling of drying (see Pakoswki and Mujumbar 2006 and Marinos-Kouris and Maroulis 2006)).

The power model proved unsatisfactory (see *Results* and *Discussion*) and the exponential model was instead selected for complete modelling and calculation of the m_{lw} values. This model was used to estimate the completely dry mass of the sample trays and the mass at 61, 62, 63 and 66 days (when groups of samples were removed for commencement of mass gain measurements), with the difference between these two amounting to the potential remaining moisture that could be removed upon heating at 500°C. Uncertainties at the 95% confidence level were calculated from the upper and lower bounds on the model coefficients estimated in *MATLAB*.

2.3 Thermogravimetric Mass Spectrometry

TG-MS was carried out using a *Netzsch TG 209 F1 Libra* thermo-microbalance in series with a *Pfeiffer Thermostar* mass spectrometer. Approximately 30-40mg of powdered dating sample (<63μm) was used. The samples had previously been dried at 130°C and stored in a desiccated environment for a period of three months. The sample was placed in an Al_2O_3 crucible within the *TG 209* and heated from 25°C to 1000°C at a rate of 20°C/min under a constant flow of nitrogen at 50mL/min. Mass spectrometry was carried out for ions of mass number 18 (H_2O), 44 (CO_2) and 64 (SO_2), liberated during the heating process. Sampling of the mass and ion current (mass spectrometry) was carried out for each °C increment in temperature.

Analysis (identification of events and structures) of the mass loss curve, its first derivative, and ion fragment curves was carried out after smoothing (typically a moving average with $n = 11$).

2.4 Carbon Content and Organic Matter Mass

Carbon content analysis was carried out at the *^{14}CHRONO Centre* at Queen's University Belfast. For each dating sample, carbon content analysis was carried out on two subsamples of approximately 0.5g powdered form (<63μm); one sample that had been dried at 130°C and another that had been fired at 500°C (these subsamples came from powdering of remaining (typically 10-20g) homogenised sample material not used in dating). Samples were combusted (in the presence of copper oxide and strips of silver) in quartz-glass tubes at 850°C for 8 hours. Then the

sample was opened into a cryogenic separation line and the CO_2 gas pressure in a specific volume recorded and converted to a mass of carbon using a laboratory conversion factor. The ratio of the mass of carbon to the original mass of the sample was used to calculate the %wt C (carbon).

For each dating sample, this provided two values, the %wt C for the sample dried at 130°C (corresponding to mass m_{c130+}) and the %wt C for the sample heated at 500°C (corresponding to mass m_{c500+}). To obtain the %wt C removed from a sample during heating between 130-500°C (m_c) the following equation was used:

$$m_c = m_{c130+} - m_{c500+} \qquad \text{(d)}$$

As part of dating trials (Barrett 2015, 2015b), before the age of the ceramic could be calculated an estimate of the organic matter mass, m_{om}, removed during reheating must be subtracted from the total mass loss during reheating. In order to do this the carbon content must be multiplied by an *organic matter to organic carbon* ratio, *OM/OC*:

$$m_{OM} = OM/OC \times m_c \qquad \text{(e)}$$

For age calculations, a standard value of 1.95 was used for *OM/OC* across all samples. For assessment of the effect of variation in the *OM/OC*, a range of 1.4-2.5 was used (Pribyl 2010; see Barrett 2015 *Section 2.5* for a summary review of the literature upon which these values were selected).

2.4 FTIR and XRD

FTIR analysis (Russell and Fraser 1994) was carried out using a *PerkinElmer Spectrum One*. For each dating sample, two powdered subsamples (< 63 μm) were prepared into pressed pellets, a sample that had previously been dried at 130°C (3 months) and a sample that had been fired at 500°C (for 18 hours). This was achieved by mixing approximately 2-5mg of sample with 40-100mg of potassium bromide (KBr) and compressing the pellet in an evacuated die under high pressure (10 tons) to form a pressed disc of diameter 13mm and thickness <1mm. These discs were then dried in an oven at 130°C for a minimum of 3 hours to remove any loosely bound surface adsorbed water before being placed in a desiccated jar to cool. Scans were then run on room temperature samples over the wavenumber range 450cm^{-1} – 4000cm^{-1}. The *Spectrum One* software was used to carry out a baseline correction on each of the scans.

Using *MATLAB*, the second derivative of the FTIR spectrum and a smoothed version of this second derivative (using *cftool* and a smoothing spline with smoothing parameter 0.0133) were acquired. The main absorption peaks were identified through comparison of the FTIR scan and its 2nd derivative with the mineral identification (carried out largely over the region 1500-450cm^{-1}) using tables compiled from the following references: Benedetto et al. 2002; Chukanov 2014; Russell and Fraser 1994; van der Marel and Beuterspacher 1976.

Special attention was also paid to the region 3000-2800cm^{-1} where absorption peaks associated with organics were compiled and tabulated.

XRD analysis was also carried out on powdered (<63μm) subsamples of both dried (130°C for 3 months) and reheated (500°C for 18hrs) dating samples. Approximately 1-2 g of powder, enough to fill a 16mm diameter holder of depth 2.4mm, was required per subsample. X-ray diffractometry was then carried out with a *PANalytical X'Pert Pro* system using Cu-Kα radiation. Scans were run over the range 3-63° (2θ) with a step size of 0.0170 (2θ) and scan step time of 120s (total scan time of 58 minutes per sample).

Analysis of the XRD spectra (Moore and Reynolds 1997) was carried out using the powder pattern analysis tool *PANalytical X'Pert Highscore Plus* (Highscore 2015). The spectra had the following treatments carried out in the following order: background removal; smoothing (quantic polynomial over a window size of n=15); peak search (using the minimum of the 2nd derivative method and a minimum peak significance of 15 counts); convert FDS to ADS correction; search and match algorithm to identify the possible minerals present using the *International Center for Diffraction Data* (ICDD) library *PDF2*. Identification of minerals present was based on both peak and profile matching with the library spectra available.

3. Results

3.1 Drying, Loose Water and Effects

The goodness-of-fit results (R^2 and *RMSE*) of the application of both drying models to the drying mass curves are presented in *Table 1* with examples of the modelled fits displayed in *Figure 1* for both *well behaved* (*Joy, top*) and *abnormally* (*Lan, bottom*) behaved samples. The terminology 'well behaved' and 'abnormal' samples corresponds to samples that displayed mass gain curves that were well suited (a clear *Stage* 2 behaviour that is linear as a function of

178 $t^{1/n}$ together with an Arrhenius temperature dependence for the mass gain rate) or poorly suited for age estimate
179 modelling; this is discussed in the companion article (Barrett 2017a). Differences in the goodness-of-fits between the
180 two drying models are minor and alone are not significant enough to merit giving preference to either model.

181 To further examine the strength of both models, the modelled loose water content, as a fraction of the modelled dry
182 mass, was correlated against properties of the ceramic that would be expected to have a strong/moderate relationship
183 with moisture content (%wt. loss between 50-130°C from TG-MS results, BET surface area and pore volume (Barrett
184 2015; 2017a; 2017b, see also *Table S3*)), *Table 2*, and provide stronger support for the use of *Model 2*.

185

186

187 **Table 1: Comparison of goodness-of-fit estimates for two models applied to drying curves of dating samples.**

	Model 1 $(m(t)=a(t^b)+c)$		***Model 2*** $(m(t)=a(exp^{-bt})+c)$	
	R^2	***RMSE (g)***	R^2	***RMSE (g)***
Ann	0.67	0.008	0.66	0.008
Esp	0.16	0.006	0.17	0.006
Nic	0.72	0.008	0.71	0.008
Mac	0.90	0.009	0.93	0.009
Ria	0.96	0.008	0.95	0.008
Etr	0.81	0.025	0.90	0.025
Rom	0.82	0.016	0.82	0.016
Por	0.90	0.017	0.94	0.017
Rat	0.89	0.006	0.89	0.006
Cal	0.95	0.007	0.94	0.007
Lan	0.72	0.016	0.79	0.016
Joy	0.96	0.008	0.95	0.008
Cau	0.78	0.008	0.83	0.008
Bel	0.90	0.013	0.93	0.013
Dow1	0.81	0.017	0.89	0.017
Dow2	0.91	0.009	0.93	0.009
Tur	0.92	0.009	0.91	0.009
Ted	0.86	0.008	0.91	0.008

188

189

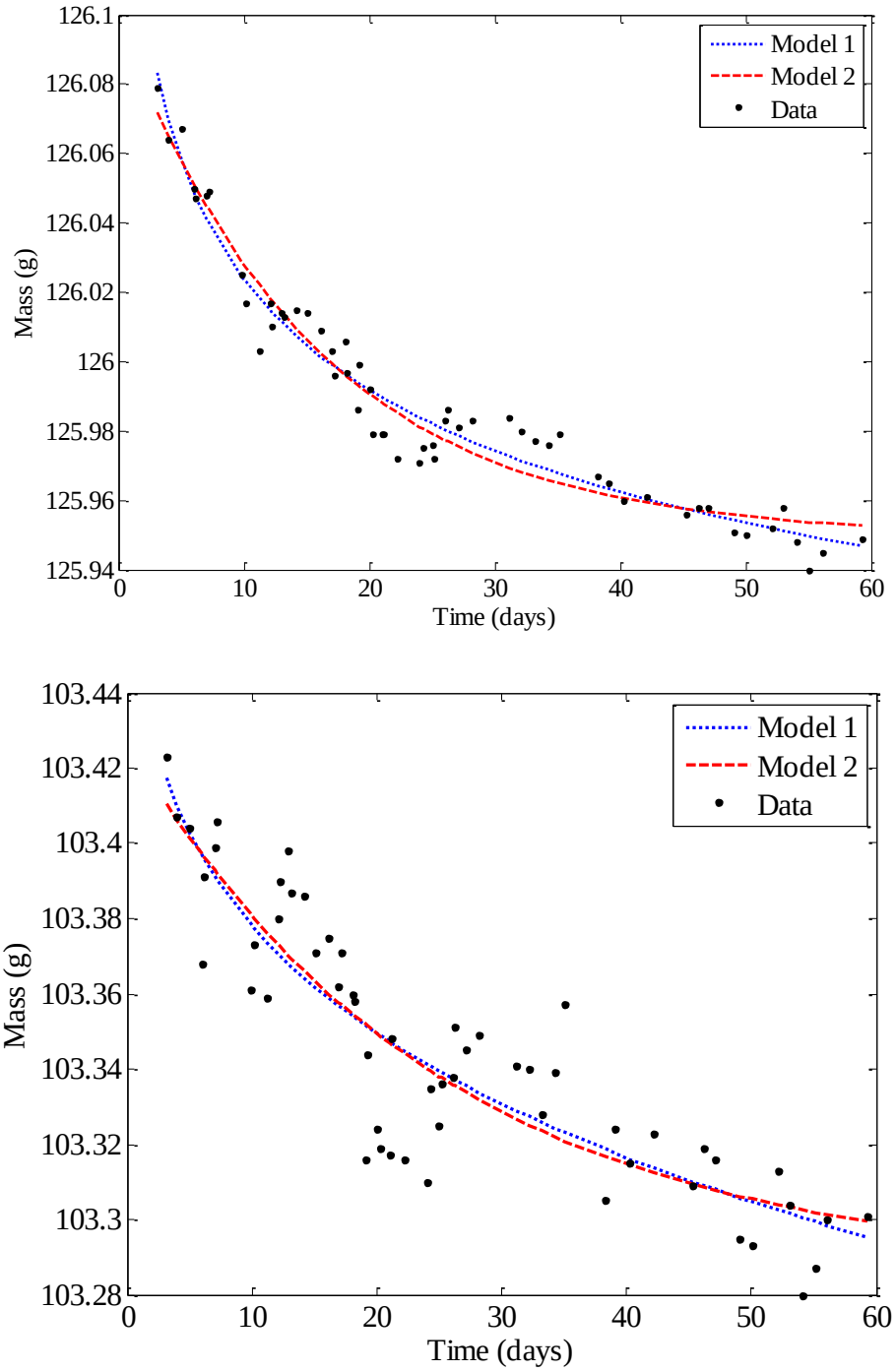

Figure 1: Drying mass curves for *Joy* (*top*) and *Lan* (*bottom*) with two models applied. Red dashed = exponential model; blue dotted = power model.

Table 2: Assessment, for both drying models, of the level of correlation (R^2) between the remaining water content (as a fraction of the estimated dry mass) and various proxies for the potential moisture content of the sample (BET S. A. and pore volume from Barrett 2015). From linear regressions carried out across all dating samples.

versus	TG-MS 50-130°C %wt loss	*BET Surface Area*	*Pore Volume*
Model 1 (R^2value)	0.11	0.04	0.10
Model 2 (R^2value)	0.53	0.38	0.43

The modelled loose water content remaining in the dried samples, after 60 days drying and given as a percentage of the modelled dry mass, is presented in *Figure 2* and arranged in order of dryness with 95% confidence intervals included also. It is notable that many of the samples with the largest values of loose water are samples (*Etr*, *Lan*, *Dow1/2*,*Por*, *Mac*,*Bel*) considered problematic in related work due to having a high specific surface area (*Table S.3*) that results in potential capillary condensation issues (Barrett 2015; 2017b). The sample *Esp* is significant as it appears to be the only sample to have dried out.

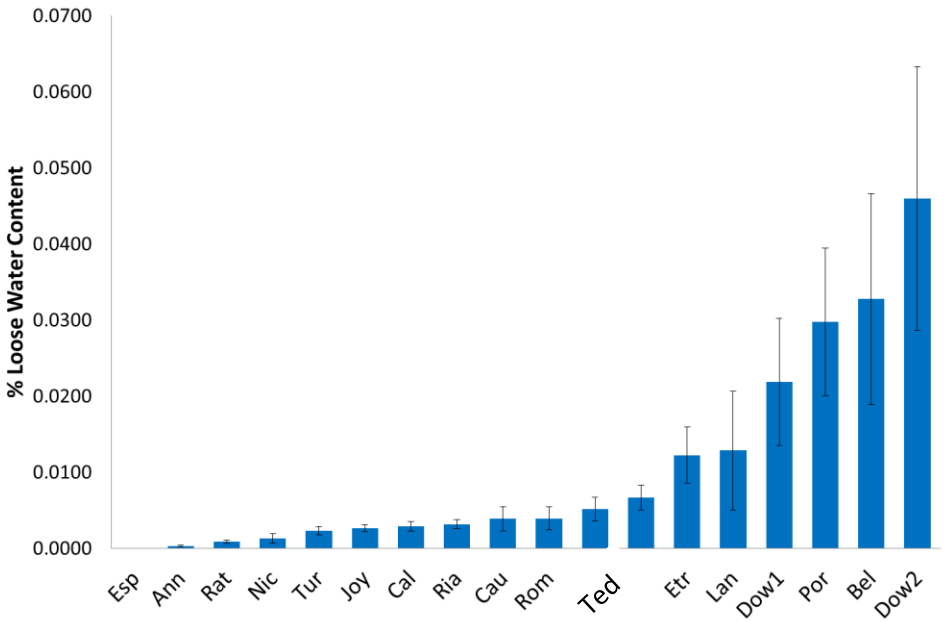

Figure 2: The modelled loose water content, as a percentage of the modelled dry mass of samples (*Model 2*), remaining after 60 days drying at 130°C. Arranged in order of dryness and with 95% confidence intervals.

For examination of the implications with regard to RHX dating, the mass of loose water, m_{lw}, is presented as a percentage of the total mass loss, m_{RHXC}, during reheating at 500°C (with regard to application of a $t^{1/4}$ model; similar

results apply to a $t^{1/n}$ model), *Figure 3*. These values vary, typically, between 0.25-1.5% but with an exceptionally high value of 3.2% (*Bel*, $t^{1/4}$ model) also obtained.

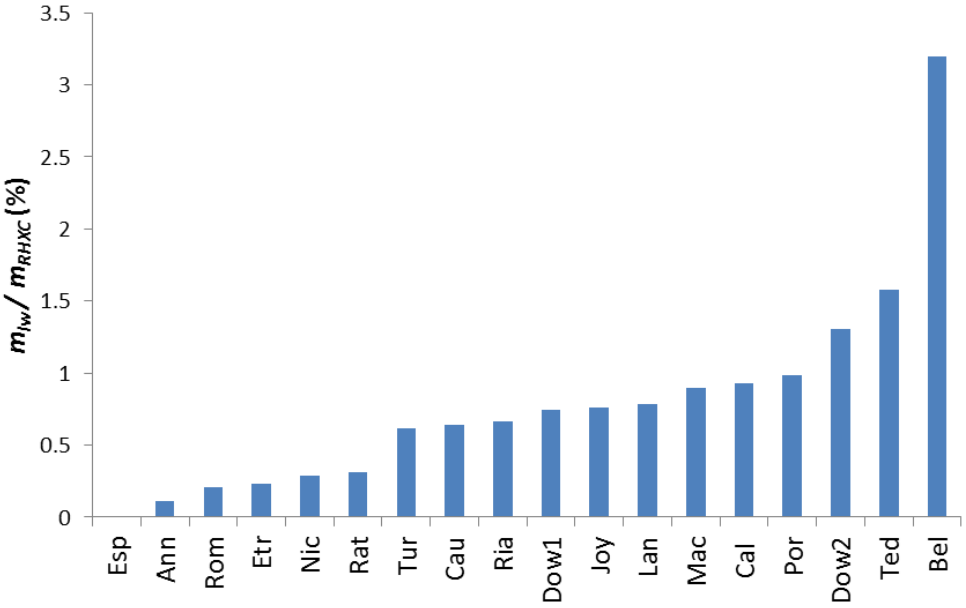

Figure 3: The mass of remaining loose water, m_{lw}, as a % of total fractional mass loss, m_{RHXC}, upon heating between 130°C and 500°C. For $t^{1/4}$ model.

3.2 TG-MS

The full set of TG-MS curves are provided in Barrett (2015). A summary of the TG-MS features observed are presented in *Table 3*. To illustrate the main heating events in this table associated with CO_2 (organic/inorganic carbon) loss, *Figure 4* presents the mass spectrometry curve for mass 44 (CO_2) with events E-G labelled. The CO_2 associated events occur over the temperature regime 200-800°C and are classified as follows:

E: *200-300°C* – onset of organic CO_2 mass loss.

F: *400-500°C* – organic CO_2 peak ('increasing' implies peak not clear due to overlap with inorganic peak.

G: *600-750°C* – inorganic CO_2 peak (carbonates).

Table 3: Summary of TG-MS analysis. Significant peaks (corresponding to events *A*-*D*) where weight loss is attributed to H_2O loss are colour coded according to strength of visible structure (all numbers are in °C). Onset of organic CO_2 mass loss (event *E*) and organic CO_2 maximum (event *F*) are included ('increasing' implies no

clear peak and overlap with inorganic calcite-related peak) together with position of inorganic carbon (calcite-related) peak (event *G*). The presence/absence of SO_2 removal is also provided.

	H_2O peaks (yellow = weak, orange = medium, red =strong)				CO_2 onset	Organic CO_2 max.	Inorganic CO_2 max.	SO2 (a=absent; p=present)
Event	***A***	***B***	***C***	***D***	***E***	***F***	***G***	
Ann	70	130	-	310	250-300	450-500	620	a
Esp	60-70	110	260-270	-	250-300	increasing	610-620	a
Nic	50	-	210-230	-	250-300	400	690	a
Mac	90	-	-	310-320	200-250	410-420	trace	p
Ria	50	120-160	-	320-330	250-300	450-500	610-620	a
Etr	90	-	240	-	200-250	increasing	730-740	a
Rom	90-100	-	230-240	-	250-300	450-500	740-750	a
Por	60-70	-	-	310-340	250-300	increasing	710-720	a
Rat	60	160-170	-	350	250-300	450-500	600-610	a
Cal	60	140	-	340-350	300-350	430-450	630-640	a
Lan	90	-	210	350-400	300-350	increasing	640-650	a
Joy	60	150	-	310-320	250-300	-	630	a
Cau	70	130-140	270-280	-	250-300	450-500	640-650	a
Bel	90-100	-	250-300	-	230-250	480	680	p
Dow1	80-90	-	200-250	340-390	250-300	370	730-740	a
Dow2	95-110	-	-	350-400	250-300	480-530	750	a
Tur	60-70	140-160	-	310-330	250-300	450-500	570-580	a
Ted	-	170-180	-	290-310	270-300	450	650-670	a

All samples featured loss of organic carbon. No inorganic carbon peak was observed for *Mac*. The presence of SO_2 was observed for *Mac* and *Bel* with SO_2 removal occurring above 650-700°C.

Four typical examples of the mass loss due to CO_2 (organic and inorganic) are presented in *Figure 5*. Clear onsets for CO_2 loss occur in the region 250-350°C, typically, with a plateau of emission common from 450°C until mass loss associated with carbonates commences from 650-700°C (the association of this peak with carbonate minerals is due to their presence in XRD, FTIR and petrography and is expanded upon in Barrett 2015). The curve for *Mac* (top right) is included as it demonstrates only a trace amount of CO_2 associated with carbonate breakdown.

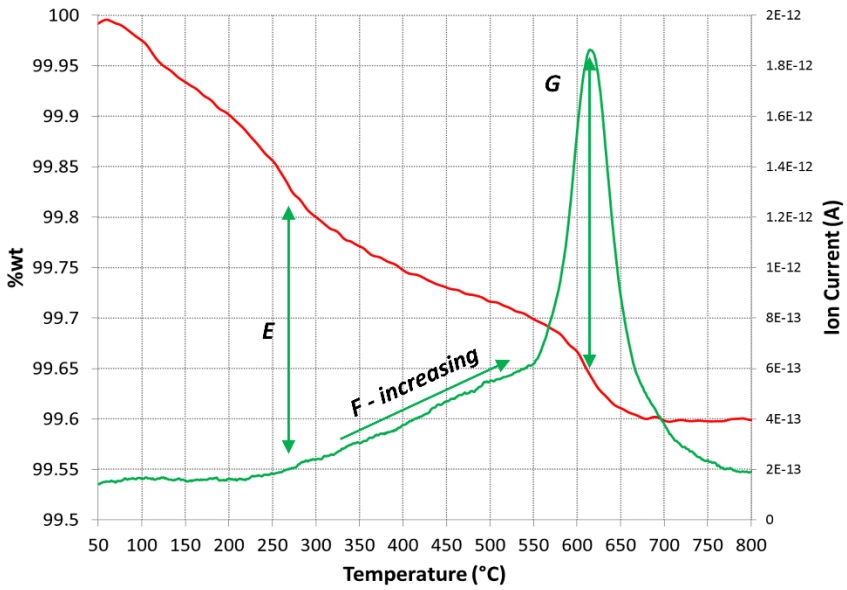

Figure 4: TG mass loss curve (red) and mass 44 (CO_2) mass spectrometry curve (green) for *Esp*. Events *E-G (see text)* are highlighted.

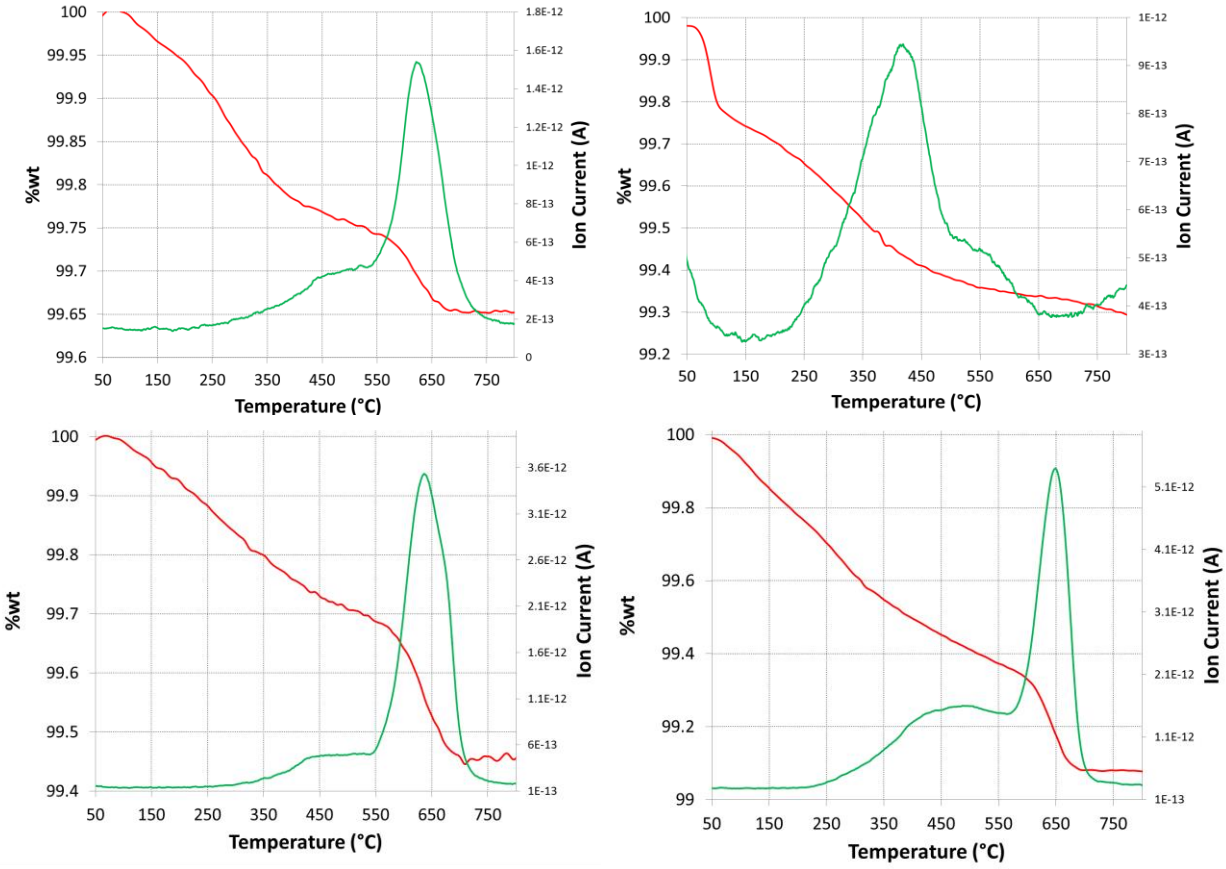

Figure 5: TG mass loss curves (red) and mass 44 (CO_2) mass spectrometry curves (green) for *Ann* (top left), *Mac,* (top right), *Cal* (bottom left), *Cau* (bottom right).

3.3 Carbon Content

The results of carbon content analysis are provided in *Figure 6*, presented as %wt C. It can be observed that that the magnitude and presence of carbon is not related to whether or not the sample was retrieved from a buried context.

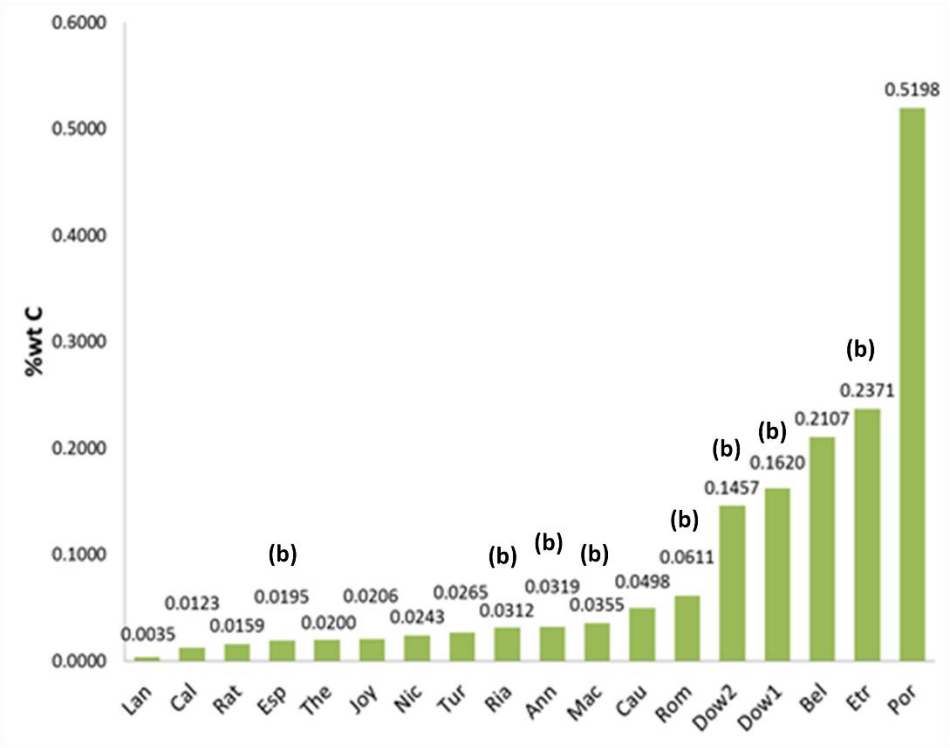

Figure 6: Percentage weight of carbon removed from dating samples during firing at 130-500°C. The retrieval of the sample from a buried context is indicated by (b).

The mass of organic matter (computed using m_c and an OM/OC ratio of 1.95), m_{om}, as a % of the total fractional mass loss, m_{RHXC}, of dating trial samples (Barrett 2015;2017a) is presented in *Figure 7* (for $t^{1/4}$ model, similar levels for $t^{1/n}$, see Figure 5 of Barrett 2017a). Levels of 5-20% are common with some values also in the range 35-45%.

The effect uncertainties in the OM/OC multiplicative factor (1.4-2.5) have on the age estimates from dating trials are displayed in *Table 4*, for both the $t^{1/4}$ and $t^{1/n}$ models. For the examples *Joy* and *Ann*, age-temperature curves, which display the age estimations as a function of effective lifetime temperature (ELT), are provided in *Figure 8* (see Barrett 2017a for details and Barrett 2015 for full set of curves).

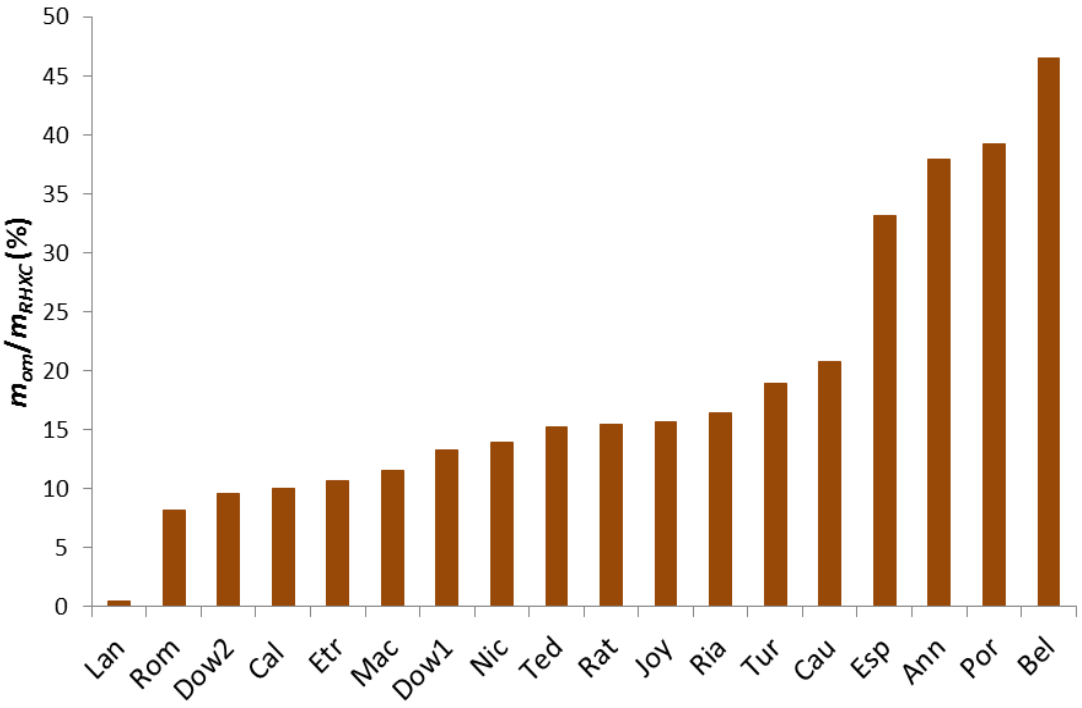

Figure 7: The mass of organic matter (computed using m_c and an OM/OC ratio of 1.95), m_{om}, as a % of total fractional mass loss, m_{RHXC}, upon heating between 130°C and 500°C. For $t^{1/4}$ model.

Table 4: Examples of the effect of uncertainties in OM/OC ratio (using 2.5 or 1.4) on the age range estimates. For $t^{1/4}$ and $t^{1/n}$ model. Italicised and bold correspond to age ranges that overlap with known age.

		Age Range (Yrs) (OM/OC) $t^{1/4}$		Age Range (Yrs) (OM/OC) $t^{1/n}$	
	Known Age (Yrs)	OM/OC (2.5)	OM/OC (1.4)	OM/OC (2.5)	OM/OC (1.4)
Ann	**110±14**	319	1283	***59***	***182***
Esp	**141 ± 6**	***147***	***452***	284	1115
Nic	**398 ± 2**	46440	66885	820437	1267480
Mac	**228 ± 2**	477321093	642239904	8113299	10271317
Ria	**339±25**	122179	191242	4150	5660
Rat	**245 ± 2**	1415987	2145539	4343	5517
Cal	**182 ± 9**	2337	3014	***177***	***212***
Joy	**412 ± 2**	***321***	***489***	152	208
Cau	**399 ± 4**	***388***	***704***	--	--
Bel	**395 ± 3**	***258***	***2178***	774	17058
Tur	**229±35**	36508	62139	359	494
Ted	**339±25**	174	263	16	21

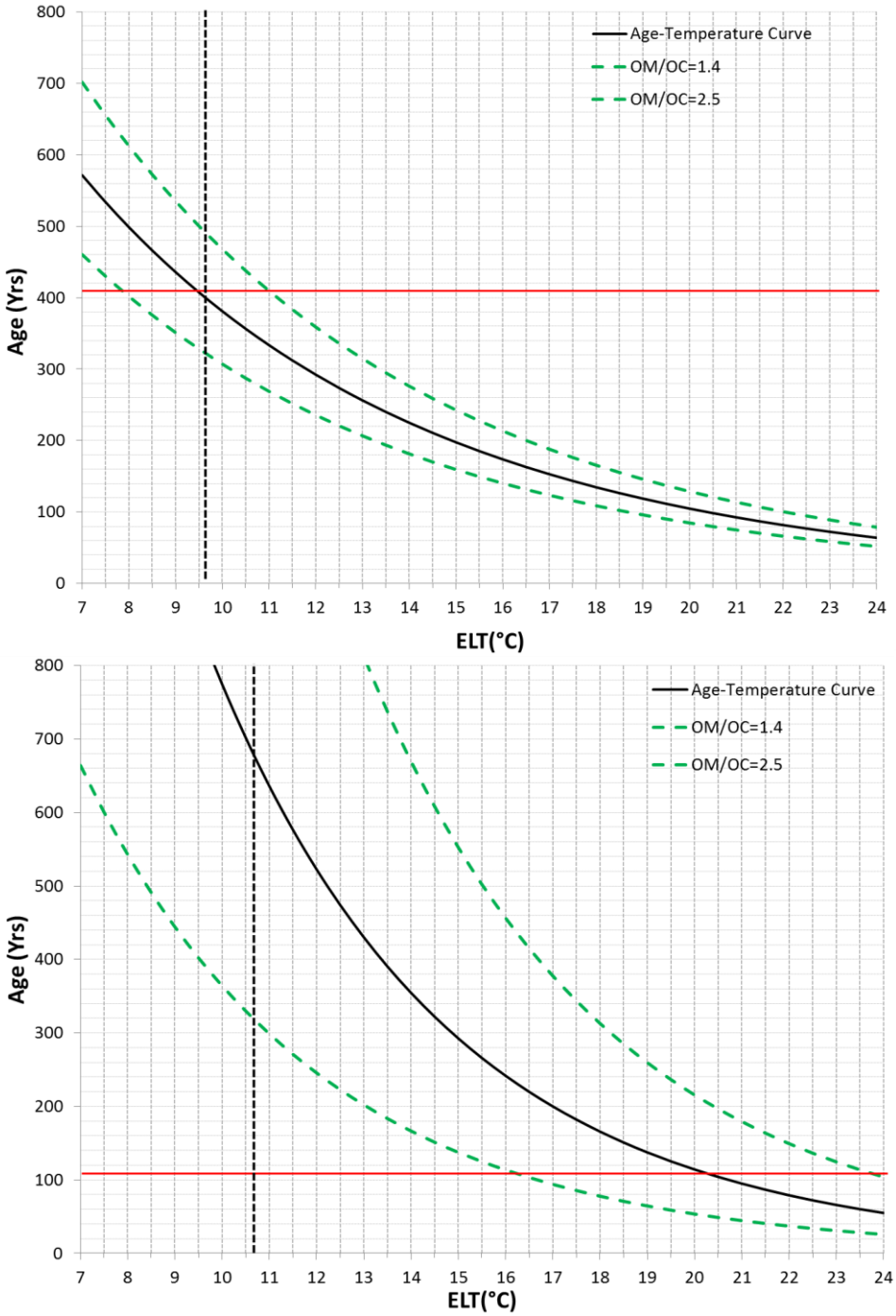

Figure 8: Effect of uncertainties in OM/OC ratio (1.4-2.5, green dash) on the age temperature curves of *Joy* (top) and *Ann* (bottom). Red line is known age. Black dashed line is ELT estimate. Using a $t^{1/4}$ model.

3.4 FTIR/XRD

3.4.1 Reheating Mineral Alteration

The complete collection of spectra with tables of peak and mineral identification for all samples using both XRD and FTIR are provided in Barrett (2015). With the exception of two samples, *Mac* and *Bel*, the spectra from XRD and FTIR showed no signs of mineral alteration associated with reheating, see *Figure 9* for *Ann* for the typical level of similarity in the reheated and non-reheated spectra.

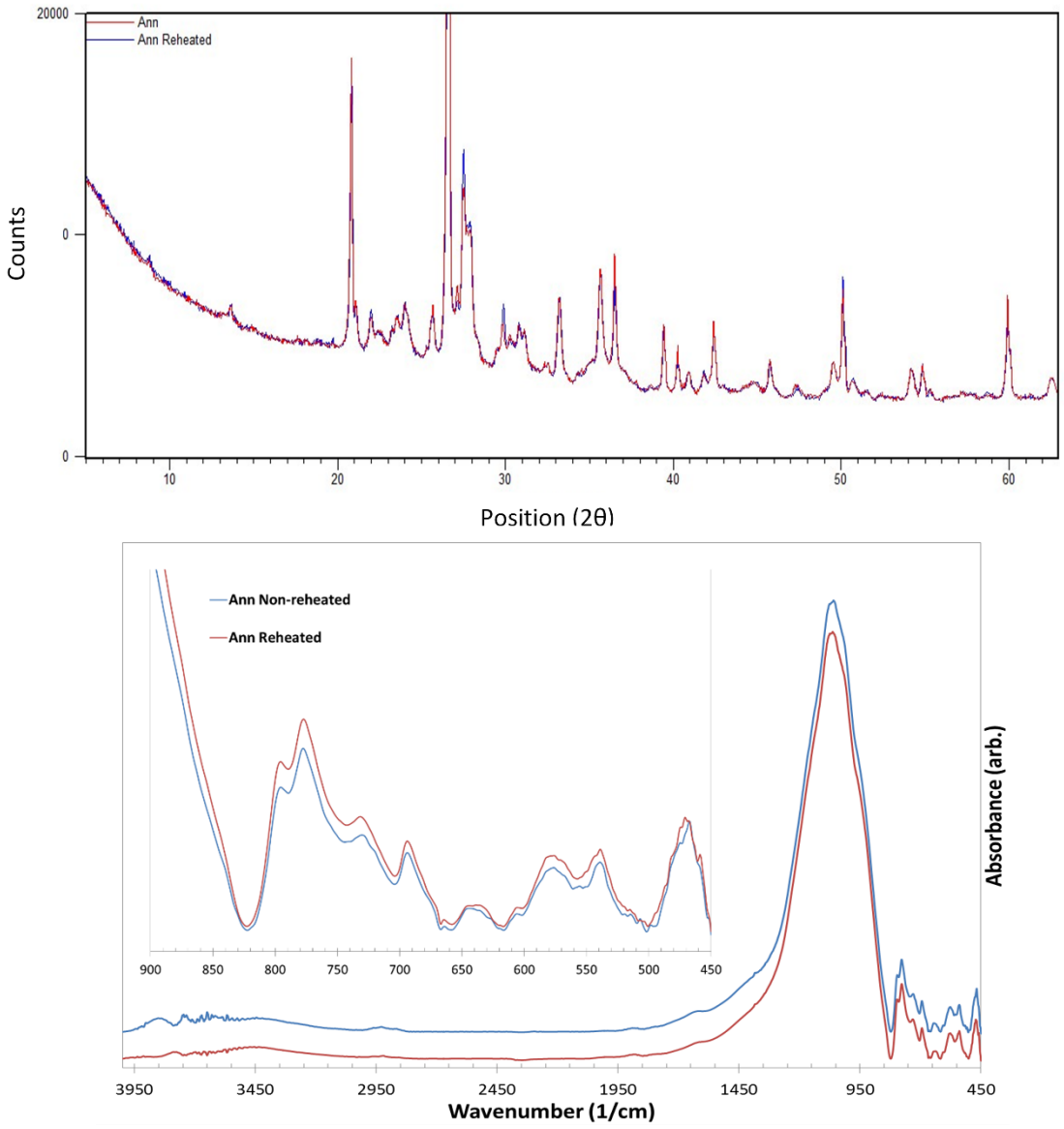

Figure 9: XRD (top) and FTIR (bottom) Spectra of non-reheated and reheated *Ann* sample. Inset of the region 450-900cm^{-1} used in mineral identification.

Two samples, *Mac* and *Bel*, displayed significant differences in spectra, with *Figure 10 (top)* for *Mac* representative of the major XRD differences observed in *Bel* also. For *Mac*, the XRD spectrum of non-reheated sample has peaks at 14.7°, 29.7° and 31.8° (2θ) that are either non-existent or very weak in the reheated sample spectrum, whereas the reheated sample spectrum has peaks at 25.4°, 38.6°, 48.6° and 52.3° (2θ) that are either non-existent or significantly weaker in the non-reheated sample. The former non-reheated peaks have been identified as bassanite (hemihydrate) reflections and the latter reflections in the reheated samples are attributed to anhydrite (using ICDD PDF2 peak identification library). Differences in the two spectra are attributed to the level of hydration of sulfates within the ceramic. For *Bel*, there are strong differences in the non-reheated and reheated spectra. The following peaks are present in the non-reheated and either absent or very low-level in the reheated sample: 14.6°, 29.6°, 31.8°(2θ). These can all be identified with bassanite (hemihydrate). For the reheated sample, peaks not present in the non-reheated sample are: 24.1°(2θ), 25.4°(2θ), 31.3°(2θ), 38.6°(2θ), 40.8°(2θ) and 41.6°(2θ). These can all be identified with anhydrite. The differences are similar to those recorded for *Mac*.

This is supported by the FTIR spectra, shown for *Mac* in *Figure 10 (bottom)* and representative of the differences observed for *Bel*. There are some significant differences between the non-reheated and reheated *Mac* samples. The reheated sample has peaks at 575cm^{-1} and 614cm^{-1} that are either very weak or not present in the non-reheated samples as well as a peak at 677cm^{-1} that appears to be greater in magnitude and shifted from 673cm^{-1} in the non-reheated sample. The non-reheated sample has a peak at 633cm^{-1} that is not present in the reheated sample together with the previously mentioned shifted peak at 673cm^{-1}. The following minerals can be attributed to the aforementioned peaks: Anhydrite = 575, 614, 617, 673, 677cm^{-1}; Bassanite = 633cm^{-1}. The change upon reheated is associated with dehydration of sulfates (gypsum).

For *Bel*, peaks at 663cm^{-1}, 669cm^{-1} and 1154cm^{-1} in the non-reheated samples are consistent with bassanite, gypsum and bassanite, respectively. Peaks at 613cm^{-1} and 678cm^{-1} in the reheated sample are attributed to anhydrite. There are no other significant differences between the spectra aside from those associated with variations in adsorbed moisture and atmospheric carbon dioxide.

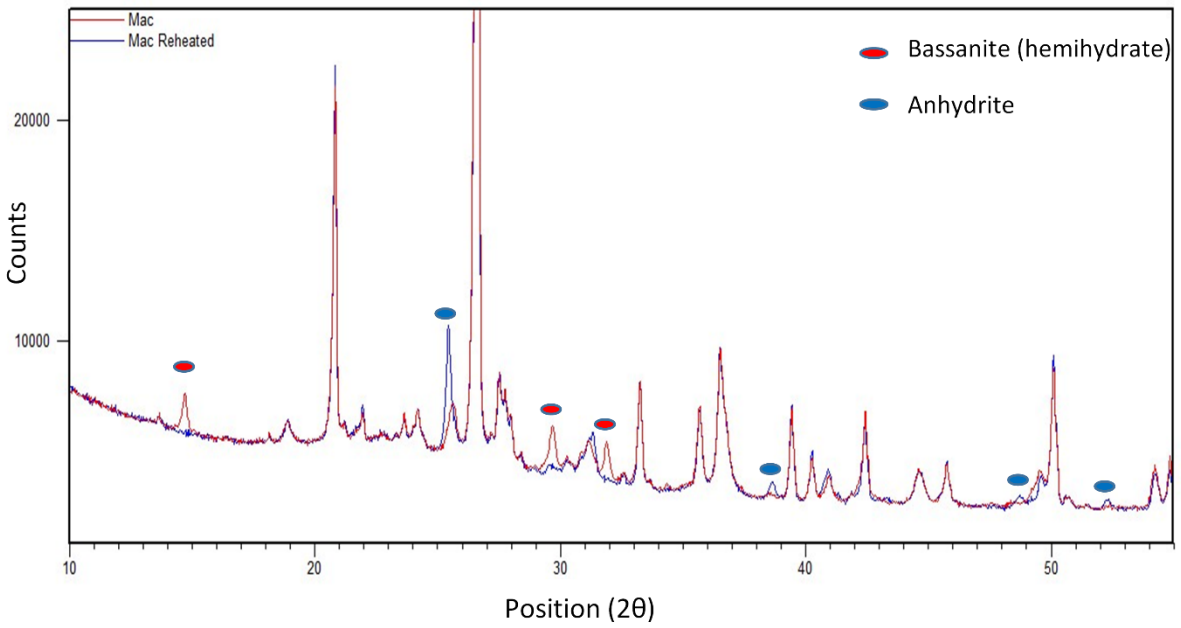

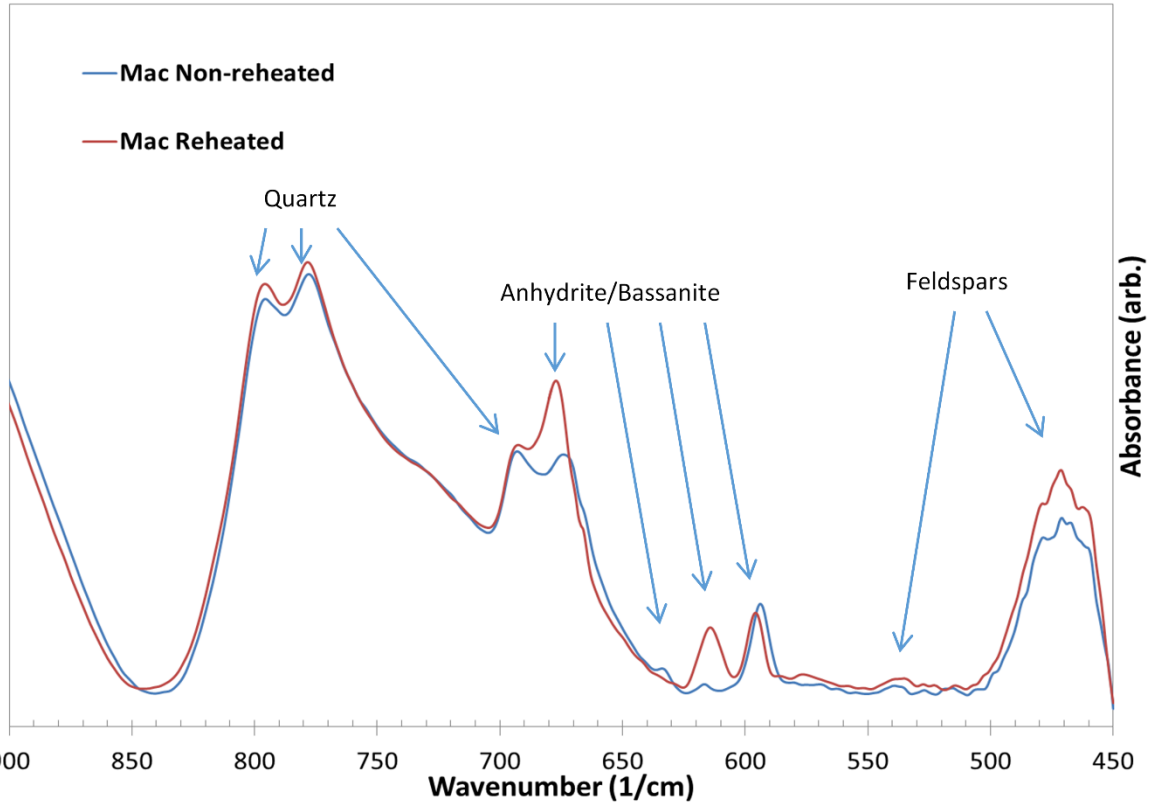

Figure 10: Top - XRD spectra of *Mac* sample without (red) and with (blue) reheating at 500°C. Region constrained to 10-55° (2θ). Red ovals mark basanite (hemihydrate) peaks; blue ovals mark anhydrite peaks. Bottom - FTIR spectra of non-reheated (blue) and reheated (red) *Mac* sample over the region 450-900(1/cm). Gypsum associated peaks (anhydrite/bassanite) are highlighted together with some examples of quartz and feldspars.

3.4.2 TG-MS Gypsum

The TG-MS measurements provided evidence for release of SO_2 only for samples *Mac* and *Bel*, see *Figure 11* for *Bel*, and with an onset above 650-700°C.

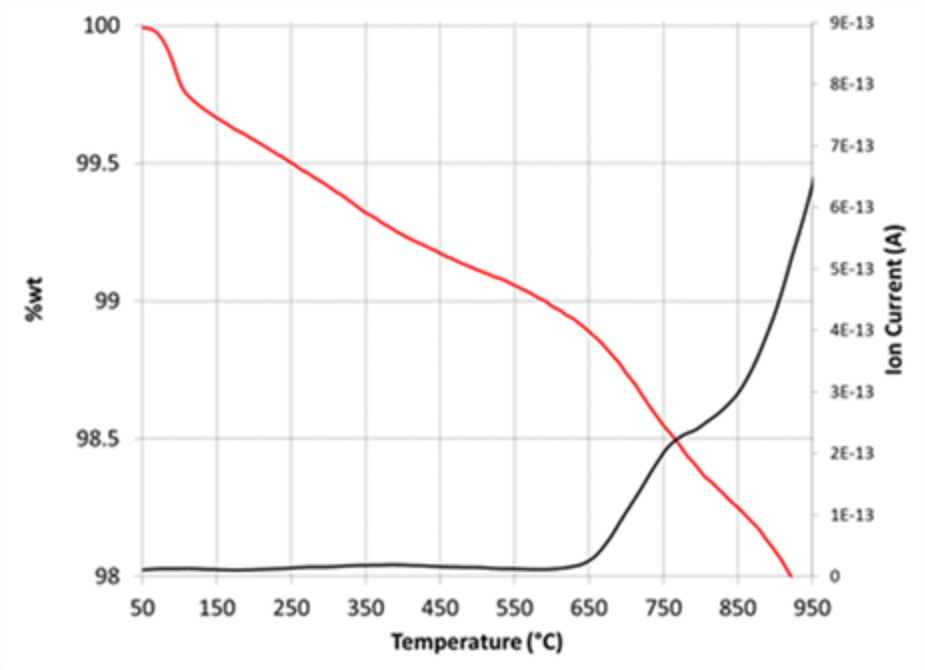

Figure 11: TG mass loss curve (red) and mass 64 (SO_2) mass spectrometry curve (black) for *Bel*.

3.4.3 Stage 1 Behaviour

Dealt with in Barrett (2015; 2017b) but of relevance to the present work are the *Stage 1 (S1)* portion of mass gain curves obtained following drying (130°C) and reheating (500°C) of samples. *Stage 1* corresponds to the initial and more rapid mass gain that occurs following drying/reheating and is attributed to physisorption-related processes (Barrett 2015; 2017b); *Stage 1* commences with exposure of the ceramic to moisture in the air and is considered complete with the commencement of *Stage 2*, i.e. when the mass gain curve is adequately modelled by a $t^{1/n}$ or $t^{1/4}$ model alone. For most samples, the magnitude of mass gain in this stage was very similar following both drying, $m_{S1\text{-}130}$, and reheating, $m_{S1\text{-}500}$; however, for *Mac* and *Bel*, there were considerable differences, see *Figure 12* for *Mac*. The magnitudes (fractional) are provided in *Table 5* with a difference of the order of ~ 4 evident.

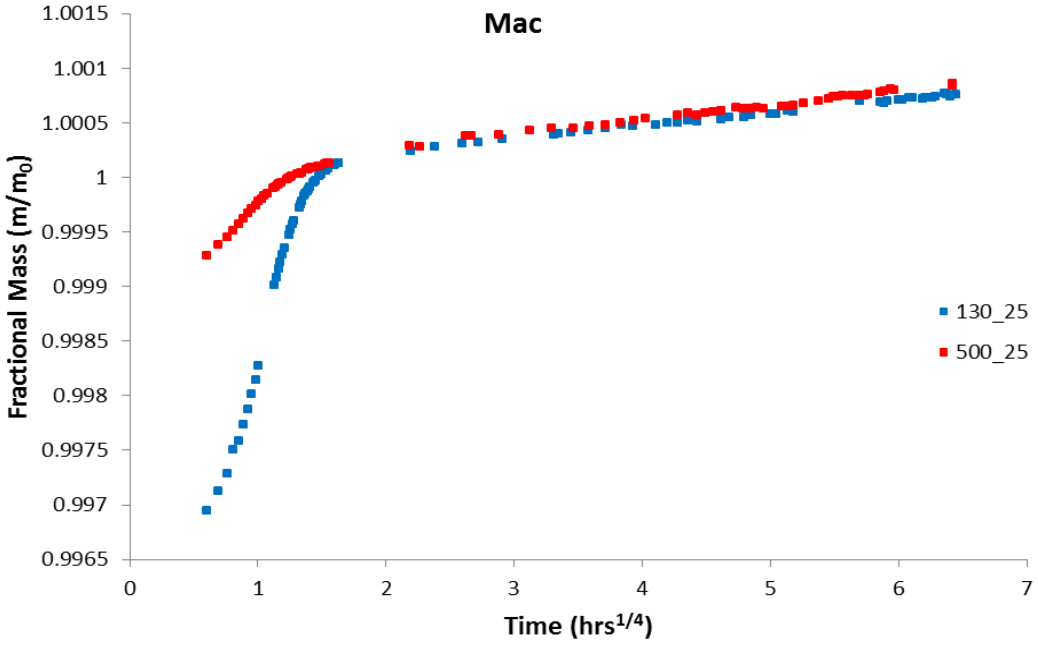

Figure 12: Fractional mass gain curves, displaying the *Stage 1* region, of *Mac* sample. Sample aging at 25°C following heating at 130°C (blue) and 500°C (red). Normalised relative to the *Stage 2* modelled intercept mass for display purposes.

Table 5: *Stage 1* fractional mass for 130C and 500C components (25°C aging) together with the ratio of the two. For the $t^{1/4}$ model (see Barrett 2015 for the method).

$t^{1/4}$	$m_{S1\text{-}130}$	$m_{S1\text{-}500}$	$m_{S1\text{-}130}/\ m_{S1\text{-}500}$
Mac	0.0030745	0.0007159	4.30
Bel	0.0048373	0.0012858	3.76

3.4.4 Organics FTIR

The results of analysis of the region 2800-3000cm^{-1} for organics are presented in *Table 6*, and *Figures 13-15*. *Table 6* presents, for all samples and for reheated and non-reheated spectra, the peak positions (cm^{-1}) and a subjective assessment of the strength of those peaks. It also attempts to group the observed peaks. *Figure 13* is a typical example of the spectra in the region of interest, 2800-3000cm^{-1}. *Figure 14* presents the peak position and their possible ranges as a function of wavenumber for non-reheated and reheated samples. Using the peak position ranges in *Figure 14*, the number of samples with organic peaks at wavenumbers from 2840-2980cm^{-1} is presented in *Figure 15*. This data is smoothed with a running average of n = 9 (cm^{-1}).

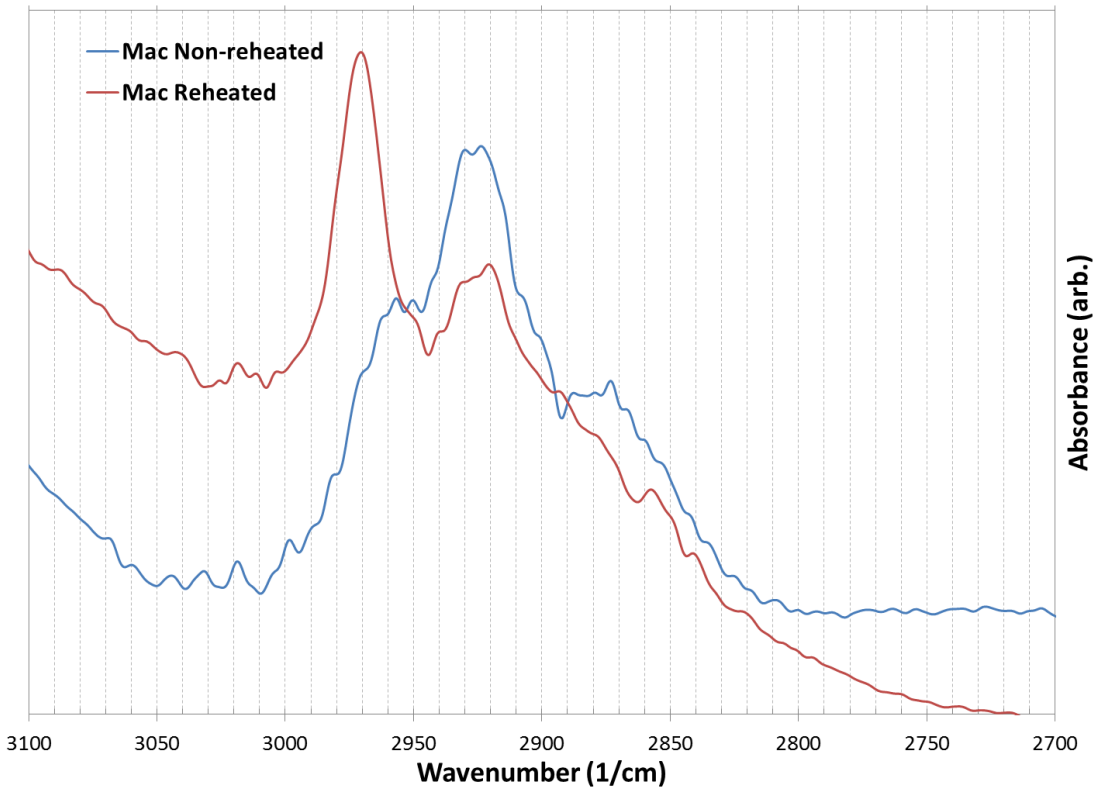

Figure 13: FTIR spectra across region of interest in organic identification for *Mac* (non-reheated and reheated). Peaks in the ranges 2850-2860cm^{-1}, 2920-2930cm^{-1}, 2950-2970cm^{-1} are typical for most samples.

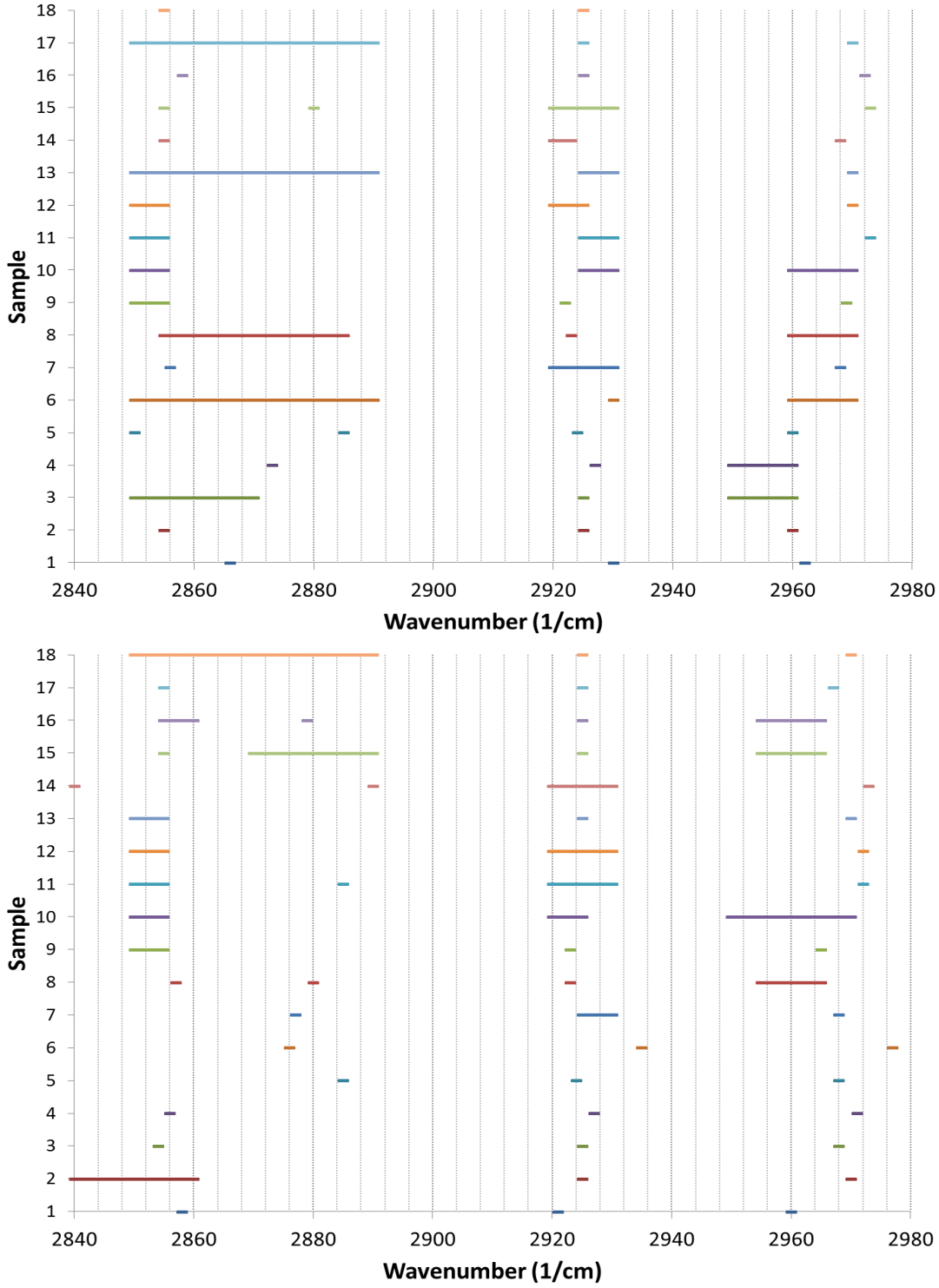

Figure 14: Peak positions of organics in non-reheated (top) and reheated (bottom) samples, see *Table 6*. Sample numbers correspond as follows: (1) Ann, (2) Esp, (3) Nic, (4) Mac, (5) Ria, (6) Etr, (7) Rom, (8) Por, (9) Rat, (10) Cal, (11) Lan, (12) Joy, (13) Cau, (14) Bel, (15) Dow1, (16) Dow2, (17) Tur, (18) Ted.

Table 6: FTIR peaks positions in organics regions 2800-3000cm^{-1} for dating samples, both non-reheated and reheated. Colour denotes relative strength of peaks: green=weak; gold=moderate; red=strong. Average values and standard deviations are based on midpoints of ranges.

	Non-Reheated				Reheated			
Ann	2866		2930	2962	2858		2921	2960
Esp	2855		2925	2960	2840-2860		2925	2970
Nic	2850-2870		2925	2950-2960	2854		2925	2968
Mac	2873		2927	2950-2960	2856		2927	2971
Ria	2850	2885	2924	2960		2885	2924	2968
Etr	2850-2890		2930	2960-2970		2876	2935	2977
Rom	2856		2920-2930	2968		2878	2925-2930	2968
Por	2855-2885		2923	2960-2970	2857	2880	2923	2955-2965
Rat	2850-2855		2922	2969	2850-2855		2923	2965
Cal	2850-2855		2925-2930	2960-2970	2850-2855		2920-2925	2950-2970
Lan	2850-2855		2925-2930	2973	2850-2855	2885	2920-2930	2972
Joy	2850-2855		2920-2925	2970	2850-2855		2920-2930	2972
Cau	2850-2890		2925-2930	2970	2850-2855		2925	2970
Bel	2855		2920-2923	2968	2840	2890	2920-2930	2973
Dow1	2854	2880	2920-2930	2973	2855	2970-2890	2925	2955-2965
Dow2	2858		2925	2972	2855-2860	2879	2925	2955-2965
Tur	2850-2890		2925	2970	2855		2925	2967
Ted	2855		2925	2965	2850-2890		2925	2970
Avg.	2859.5	2882.5	2925.4	2965.8	2855.3	2881.9	2925.2	2967.3
Std. Dev.	7.7	2.5	2.5	5.4	5.9	4.9	2.8	5.2

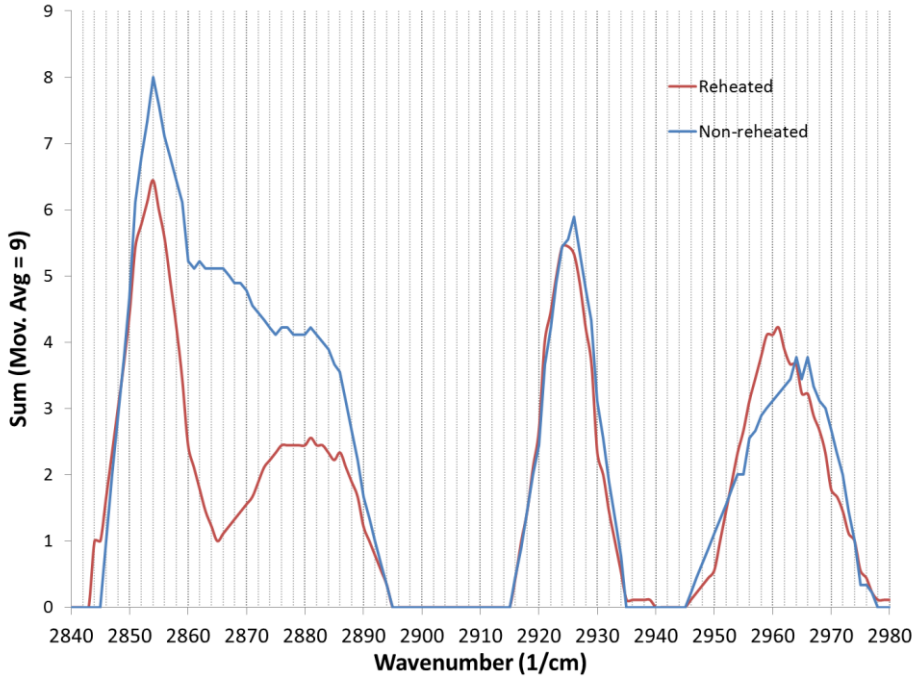

Figure 15: Moving average (n=9) of number of samples with organics peaks at wavenumbers from 2840-2980cm^{-1}, for both non-reheated (blue) and reheated (red).

4. Discussion

4.1 Incomplete Drying

Two models (power-based and exponential-based) were applied to the drying mass loss curves, *Figure 1*, with the quality of the regressions quite variable, *Table 1*. Differences between the goodness-of-fits of both models are minor and do not provide clear support for the selection of either. A better distinction might be made with improved quality data; however, this issue with prolonged drying was unexpected when the experiment was designed. Control of environmental conditions during removal from the oven for weighing was inadequate to prevent large fluctuations in the mass, associated with the level of physisorption taking place; this is reflected in the *RMSE* values of the models, *Table 1*, where samples with high surface area (*Etr, Rom, Por, Lan,* see *Table S.3*) have the largest fluctuations, see for example *Figure 1* for *Lan*.

The correlation of the modelled remaining mass of loose water with properties with which it would be expected to be associated, for example surface area and pore volume, was examined, *Table 2;* these results favour the exponential model.

The exponential model was ultimately selected for the reasons above and also because the power-based model was problematic; for a number of samples, the modelled mass of remaining loose water exceeded the mass loss estimates due to heating at 500°C, and for several samples regressions using the power-based model produced parameter values that were nonsensical (i.e. a final 'dry' mass that exceeded the initial mass of the drying curve). As well as this, the use of a power model was motivated by a $t^{1/2}$ behaviour suggested by Brosnan and Robinson (2003); however, the model could only be successfully applied with the power constraint relaxed (*1/n* instead). The exponential model is more satisfactory in its interpretation, with the rate of moisture removal being proportional to the level of moisture remaining.

While the exponential model was selected for use, the authors emphasises that this was borne out of pragmatism and the appropriateness of this model clearly requires more investigation; the quality of the fits produced, *Figure 1*, were less than satisfactory, and the confidence intervals were also very large, for example *Figure 2*. Nonetheless, its use was deemed the only way to proceed. That the modelled remaining loose water was generally greatest for the high surface area samples, *Figure 2* and see *Table S.3*, is somewhat reassuring and would also explain the greater correlation

572 of this model with the surface area, pore volume and TG-MS data, *Table 2*, the inference being that for high surface
573 area samples a significant quantity of physisorbed water is possibly still being removed when heated at 500°C.

574 **Table 7: Summary of the drying conditions and presence of drying data in the literature.**

Publication	Sample Size	Drying Temp. (°C)	Duration of Drying	Drying Data Presented (Y/N) (other drying proxy data)
Wilson et al. (2009)	3-5g	105	Not specified (to constant mass)	N
Bowen et al. (2011)	32-96g (sherd)	110	20-30hrs (However, incomplete drying after 2 weeks)	Y
Wilson et al. (2012)	0.5-4.0g	105	To constant mass ('few hours' to 'several days')	N
Bowen et al. 2013	1-2g	110	30-50hrs	N
Burakov and Nachasova (2013)	1-15g	105	12hrs	N
Le Goff and Gallet (2014)	2-3g	105	4 and 16hrs for one group 66 and 51hrs for one group Issue with duration of raised, additional mass loss with repeated heating	N (Mass gain curves demonstrating variation in mass level with drying temp. 95/105°C and duration)
Le Goff and Gallet (2015a)	2-3g	105	11hrs and 14 days	N (Mass gain curves demonstrating increase in mass gain rate ($t^{1/4}$) with prolonged drying)
Numrich et al. (2015)	2-4g	110	48hrs	N
Gallet and Le Goff (2015)	1.46-3g	60, 85, 105, 130	5hrs at 60, 85, 105, 130°C 23hrs at 105°C 246hrs at 105°C	N (Mass gain curves demonstrating extra loss in mass as a function of heating temperature and additional heating duration, with effects on mass gain behaviour also evident)
Zhao et al. 2015	0.4-1g	110 300	5-7 days at 110°C Overnight at 300°C	N

575

For all samples, excluding *Esp*, drying was incomplete after 60 days, *Figure 2*, with the potential for considerable quantities of moisture to be removed with additional drying, typically 0.25-1.5% of the total mass lost during reheating at 500°C, *Figure 3*. This poses potential issues for dating estimations where it is necessary to estimate the rehydroxyl mass loss, m_{RHX}, during heating at 500°C. If, say, up to 2% of this mass estimate is actually loosely bound physisorbed water, m_{lw}, that has not been recognized or poorly accounted for, then a discrepancy in the age estimate of approximately 8% of the age estimate can result (i.e. if there is an uncertainty, dm, in the mass, m, then the uncertainty, dt, in the age estimate, t, is given by $(t+dt)/t = ((m+dm)/m)^4$). For the associated dating trial (Barrett 2017a), the estimated m_{lw} was taken account of using the results presented in the present work. There are clearly large uncertainties in this estimation, on account of the quality of the data and uncertainty in the model used. Nonetheless, even permitting m_{lw} to contribute a maximum of 4% of the total mass loss, the result is only a 17% discrepancy in the age estimate and this, unfortunately, is still only a minor contributor to the significant discrepancies observed in age estimates (Barrett 2017a, see also *Table 4*). Ignoring the results of the dating trial, if all other issues could be removed, then uncertainties of this magnitude alone would be problematic for the validation and use the method.

Prolonged drying is clearly an issue for RHX dating; its possible presence in previous work was examined, with the conditions of drying and evidence for constant mass or long drying times summarised in *Table 7*. For the majority of these studies, samples were dried either at 105-110°C until they reached constant mass (Wilson et al. 2009; 2012) or for a fixed duration expected to be long enough to dry them out, yet without a strong rational for selection of drying times that range from a few hours to a few days (Bowen et al. 2013; Burakov and Nachasova 2013; Numrich et al. 2015). These studies used samples that are of typical size 0.5-10g, greater than the size of the individual granules used in the present work (maximum size of approx. 0.3g). For experiments where a fixed duration was used, without drying to constant mass being recorded, there is no certainty the samples actually did dry out. For the experiments where samples were stated as drying to constant mass (Wilson et al. 2009; 2012), no evidence or data to support this is presented.

There is support for the findings of the present work in the publications of Bowen et al. (2011), Le Goff and Gallet (2014; 2015a), Gallet and Le Goff (2015) and Zhao et al. (2015). Bowen et al. (2011, Figure 3) produced drying curves that demonstrated that after a period of 2 weeks drying at 100°C constant mass had still not been achieved; however, they do not pursue the matter much further and this was for relatively large samples, 32-96g. Le Goff and

603 Gallet (2014; 2015a) draw attention to the need for better understanding of the effects of drying temperature and
604 duration, finding that for longer drying times or higher temperatures there is an additional/greater mass loss
605 (observable in a shift in the subsequent mass gain curves to lower mass, see Figure B of Le Goff and Gallet (2014)).
606 Unfortunately, they do not record the mass of the samples as a function of drying time, so again it is not possible to
607 know if, even for the longest drying times used, 14 days, complete drying occurred. From Gallet and Le Goff (2015)
608 there is strong evidence that incomplete drying occurs for the duration used (5hrs) while heating at lower temperatures
609 (60, 85, 105, 130°C) with increases to the next highest temperature producing greater mass loss and mass gain rates.

610 In Zhao et al. (2015) issues with incomplete drying at 110-120°C in unpublished work is stated as prompting the use
611 of a drying temperature of 300°C.

612 In any case, from the above, there is a lack of evidence in the literature that drying to constant mass is actually
613 achieved, with evidence that it is instead prolonged (Bowen et al. 2011, Zhao et al. 2015) and poorly understood (Le
614 Goff and Gallet (2014; 2015a); Gallet and Le Goff 2015). The present work suggests that drying is a non-trivial issue
615 such that even after two months drying at temperatures of 130°C and granules of < 0.2g there is still considerable
616 potential for water to be removed.

617 As well as this, there is the question over the nature of the water being removed; is it solely physisorbed/pore/capillary
618 water that is loosely held/bound (Wilson et al. 2009; 2012) or is chemisorbed water also being removed (e.g. Gallet
619 and Le Goff 2015; Barrett 2015; 2017b), with the latter responsible for the prolonged behaviour, particularly in low
620 surface area well-behaved samples (see Barrett 2015; 2017b). If the remaining moisture not removed after 60 days
621 drying is attributed to loose water, m_{lw}, then it needs to be subtracted from the total mass loss, m_{RHXC}, upon reheating
622 at 500°C in order to obtain the RHX related mass loss, m_{RHX} (Barrett 2015; 2017a). However, this assumption of
623 drying only removing physisorbed water was originally guided by assertions that equilibration of the mass occurred
624 following drying (Wilson et al. 2009; 2012). The work of Le Goff and Gallet (2014; 2015a), Gallet and Le Goff
625 (2015) and Barrett (2015) demonstrate that this is not the case, and, further, that those assertions were not well
626 supported experimentally (Le Goff and Gallet 2015a). Instead, it seems increasingly likely (Gallet and Le Goff 2015;
627 Barrett 2015; 2017b), that the two stage mass gain behavior, with *Stage 2* described well by a $t^{1/n}$ model , following
628 drying is a chemisorption driven process and associated with the removal of chemisorbed water during drying.
629 Interestingly, this seems supported by the result that the only sample to fully dry was *Esp* for which *Event B* (TG-MS

data, *Table 3*, associated with a chemisorption process by Barrett 2015; 2017b) was low in magnitude and with a peak water removal temperature of 110°C, the lowest for samples where *Event B* was certain, and well below the drying temperature of 130°C used in mass gain tests.

If prolonged drying is associated with chemisorption (with removal of loose water completed at some earlier point) then it may not be necessary to estimate or subtract the quantity m_{lw} if the component based approach proposed by Barrett (2015; 2017) is valid. This approach will not be discussed but provided all physisorbed water is removed then the remaining chemisorbed water not removed is taken account of in its methodology. The implications of this are dealt with in Barrett (2015).

In any case, the present work demonstrates that complete drying is unlikely or impractical using simple oven based setups and highlights the need for more controlled recording of the mass loss curves during drying in order to (a) assess the quantity of loose water remaining (if drying is associated with loose water removal alone) or (b) to provide evidence that the stage associated with removal of loose water is complete, with continued mass loss due to removal of chemisorbed water. Modelling of the mass gain curves using the approaches above could be used in (a) and may be useful in observing transitions in (b).

4.2 Carbon Content

It can be observed from that carbon (organic) context was significant in all samples regardless of the context of retrieval, varying from 0.0035 – 0.5198 %wt, *Figure 6*. As well as this, there does not appear to be notably lower levels present in non-buried samples; this is made clear by the high carbon content in *Cau*, *Por* and *Bel*, and highlight that significant quantities of organic matter should be treated as plausible mass contaminants in all samples used in future RHX dating trials. It is also worth noting that the highest levels were obtained for the samples *Por, Etr, Bel, Dow1, Dow2, Rom, Cau* (0.52-0.05 %wt) and this will be returned to later. From the TG-MS data, *Table 3* and *Figures 7-8*, it is clear that at heating temperatures from 200-300°C mass loss associated with CO_2 removal commences, *Event E*, corresponding to commencement of the removal of organics (Ford 1967; Rice 1987; Dunham 1992; see Barrett 2015 for a more detailed review of mass loss temperatures associated with firing of ceramics). This removal appears to peak or plateau in the range 400-500°C, *Event F*, however is not complete until higher temperatures. This is supported by the FTIR data, *Figures 15-16* and *Table 6*, where the presence of organics peaks in region 2800-3000cm^{-1} is still strongly detected even after reheating of powdered samples (<63μm) at 500°C for 18 hours. This is an area

of concern for RHX dating where it is essential that the carbon removed during heating at 500°C equates to that measured as part of carbon content analysis.

From the FTIR identification in the region 3000-2800cm^{-1}, four main bands are identified as present in both the non-reheated and reheated samples, *Table 6* and *Figure 13-15*. This region of CH absorption was selected because it is absent of mineral interference and subjectivity issues associated with other regions (see Reeves III 2012). A possible band at 2860-2870cm^{-1}, present only in the non-reheated samples, appears to be only an effect of the broad absorption band ranges assigned to samples in *Figure 14* because of uncertainty in the peak and is not considered real. The remaining four peaks, summarised below in *Table 8*, together with infrared bond assignments and organic source interpretations, are made up of the dominant bands, 2845-2860cm^{-1}, 2920-2930cm^{-1}, and 2950-2975cm^{-1} and a lesser band at 2870-2890cm^{-1}. These bands are identified as due to bonds associated with organic matter (CH bonds), specifically aliphatic stretching and bending bonds, *Table 8* (identified using Larkin 2011). According to Larkin (2011) the aliphatic stretching bonds often appear as a pair of doublets (in phase, out of phase) and it appears that two sets of doublets are observed in the present work, *Table 6*, one associated with *R-CH_3* stretching and the other associated with *R-CH_2-R* (*R* is an unspecified group/molecule attached).

Table 8: Table of main FTIR peaks associated with organic matter, together with IR bond assignments, possible organic matter source, and associated references.

Wavenumber cm^{-1} (n=non-reheated,r=reheated)	**IR bond Assignment (Larkin 2011)**	**Suspected/Potential Source Organic**	**Reference**
1. Peak =2854 (n,r) Range=2845-2860	Aliphatic R-CH_2-R Stretching (in phase)	Humic/Fulvic Acids Peat-Anthracite (coke)	Vergnoux et al. 2011 Reeves III 2012 Madari et al. 2006
2. 2880 (n,r) 2870-2890	Aliphatic R-CH_3 Stretching (in phase)	Not Clear	--
3. 2925 (n,r) 2920-2930	Aliphatic R-CH_2-R Stretching (out of phase)	Humic/Fulvic Acids Peat-Anthracite (coke)	Vergnoux et al. 2011, van der Marel et al. 1976 Reeves III 2012 Madari et al. 2006
4. 2960,2970 (n,r) 2950-2975	Aliphatic R-CH_3 Stretching (out of phase)	Hard Coal, Brown Coal, Coke	van der Marel et al. 1976 Guisnet and Magnoux 2001

675 Possible organic sources are included in *Table 8* together with references for the identification at these bands; however,
676 no source could be assigned to the band at 2870-2890cm^{-1} and the sources for the remaining bands are by no means
677 certain. The organic matter in soils is often characterised by a double absorption band at 2855cm^{-1} and 2930cm^{-1} (e.g.
678 Madari et al. 2006; Vergnoux et al. 2011; Reeves III 2012), yet with no peak at 2950-2975cm^{-1} identified by these
679 authors. Fernandes et al. (2010) provide FTIR spectra of the organic matter, humic and fulvic, in some soils and peats;
680 again the double peak at 2855 cm^{-1} and 2930 cm^{-1} is evident yet any peak at 2950-2975cm^{-1} is absent. Chen et al.
681 (2012) carried out FTIR on a suite of coals varying from peat to anthracite and again the double peaks at 2857cm^{-1}
682 and 2927cm^{-1} were observed without any third peak apparent (this is supported by similar work by Tian et al. 2010).
683 In this regard, the strong triplet of peaks observed in this study may be more characteristic of a triplet of peaks
684 identified by van der Marel and Beuterspacher (1976) at 2950cm^{-1}, 2920cm^{-1}, and 2850cm^{-1}, found in peat, black peat,
685 brown coal, lignite, hard coal and bitumen. The presence of substances derived from the peat-to-anthracite formation
686 group is certainly possible for raw clays (Dunham 1992), yet it seems unlikely, given the high firing temperatures
687 interpreted for most of the samples (Barrett 2015), that much, if any, of these substances would survive. It is
688 conceivable that, in a reduced (oxygen deprived) firing environment within the kiln (or even within the brick), carbon-
689 rich coke may have been produced and that the major absorption triplet observed in the data could be explained by
690 similar triplet of peaks at 2860cm^{-1}, 2930cm^{-1}, and 2970cm^{-1}, as observed in Guisnet and Magnoux (2001). The use
691 of coke as a fuel in the firing of bricks (in clamps and kilns) is/was not uncommon (Hammond 1981; Brunswick 1990;
692 Pavía and Bolton 2000) and this could also be a source of contamination, particularly post-firing.

693 From the above, it can not be clarified whether the source of the organics is humic-related substances or derived from
694 part of the peat-to-anthracite formation pathway. From TG-MS, the organics are predominantly being burnt off at
695 temperatures well below the original firing temperature, i.e. less than 500°C and certainly not above 800°C, suggesting
696 that the source of organics removed during the RHX methodology are more likely to be post-firing contamination
697 from burial or air-borne/rain precipitated processes, presumably humic-related substances. That the source of organic
698 matter is likely to be post-firing contamination may be supported by findings from BET analysis, presented in Barrett
699 (2015), where the samples with highest surface area (*Table S.3*) and pore volume (with the exception of *Lan* where
700 the carbon content is very low) are also those with the highest carbon contents above (and calcite content, dealt with
701 in Barrett 2015). In Barrett (2015) the BET surface area is also highly correlated (R^2 = 0.90) with the percentage of
702 water removed in the TG-MS heating regime 50-130°C (Figure 5.34 of Barrett 2015), with the greatest quantities of

703 water loss also occurring for the samples with highest surface area and pore volume, (Figure 5.29 of Barrett 2015).
704 This suggests that high pore volume and surface area may be associated with, and permit, greater uptake of
705 environmental moisture (groundwater, rain), and with it sources of carbon and calcite contamination, supporting an
706 argument that much of the carbon content is derived from post-firing organics of humic origin.

707 It is not ideal that for each sample only a single estimate of the carbon content was carried out using two measurements
708 of the carbon content of two subsamples, one of which had been previously heated to 500°C.[1] These subsamples were
709 taken from a well-mixed powder of the remaining granules from which the dating subsamples were taken. Hence, the
710 samples used in carbon content analysis are expected to be well homogenised and representative of the dating samples
711 in their carbon content.[2] Nonetheless, variation is to be expected, and with only a single estimate carried out per
712 sample the repeatability of carbon content measurements and the associated uncertainty can not be estimated. As well
713 as this there will be sources of uncertainty in the procedure used for its estimation. However, the author worked under
714 the assumption that the uncertainties in the carbon content, associated with subsample variation and the experimental
715 method, would be minor when compared with that associated with the organic matter to organic carbon ratio; the
716 range of the OM/OC uncertainty used was 1.4-2.5, which equates to a percentage uncertainty of 28% in the mass of
717 organic matter (based on OM/OC ratio of 1.95 used in age estimates), and was considered broad enough to encompass
718 and take account of any sources of uncertainty in the carbon content. These values for the organic matter to organic
719 carbon ratios are based on a survey of research focussed on its estimation for organic matter from a range of
720 environments (aerosol-borne, soil, peats, clays), presented in *Table 9*. This survey, while not comprehensive,
721 demonstrates that the OM/OC ratio can vary considerably but for all studies falls within the range 1.0-3.0. Notable
722 attention is given to the work of Pribyl (2010) who in a review of 26 existing publications concluded that "*a*
723 *consideration of the possible variation in organic matter composition predicts a range of factor values between 1.4*
724 *and 2.5*". This range is used in the present work as an adequate, if not ideal, reflection of the range of likely ratios for
725 contaminants found in ceramics, aerosol-borne or burial-related.

[1] This was constrained by the large number of samples, 36, which needed to be prepared and analysed. Ideally, the carbon content of the subsamples used in mass gain experiments would be captured during heating at 500°C; if conducted on the three subsamples, this would also provide some useful information on the homogeneity of the samples and uncertainty in the carbon content.

[2] The XRD, FTIR, and XRF analysis has demonstrated that the two subsamples used in reheated and non-reheated tests were almost identical both mineralogically and in elemental composition.

Table 9: A short survey of the organic matter to organic carbon ratios from publications focussed on different environments/sources of organic matter.

Environment/Source	OM/OC typical value	OM/OC range
Aerosol		
Ruthenberg et al. 2014	1.69	1.4-2.15
El-Zanan et al. 2009	1.92	1.52-2.32
Phillips et al. 2014	1.5 (urban)	not clear
	2.0 (rural)	not clear
Turpin and Lim 2001	1.6 (urban)	1.4-1.8
	2.1 (non-urban)	1.9-2.3
Soil		
Pribyl 2010 (*Review*)	Soil	
Soil	2.0	1.4-2.5
Humin	-	1.49-1.61
Humic Acid	-	1.70-1.85
Fulvic Acid	-	1.96-2.44
Carbohydrate	-	2.22-2.5
Lipids	-	1.27-1.45
Amino Acids	-	1.54-3.0
Peats		
Klingenfuß et al. 2014		
Own Work	1.73-2.41 (dependent on peat type)	1.64-2.97
Review of existing work	-	1.55-2.31
Clays		
Worrall 1956		
Ball Clays	1.56	1.51-1.61
Fireclays	1.26	1.15-1.37

The mass of organic matter, m_{OM}, is a considerable fraction (5-20% typically for better behaved samples on which dating attempts could be made, see Barrett 2015; 2017a) of the total mass loss, m_{RHXC}, during reheating, *Figure 7*, and is subtracted (along with loose water, for example) from this quantity in order to obtain the RHX mass used in age estimations, m_{RHX}. Therefore, the range of uncertainty used for the OM/OC ratio has a considerable effect on the estimated ages of the samples, *Table 4* and *Figure 8*, causing an uncertainty in the age range of a minimum of 35yrs (for *Cal* and $t^{1/n}$) but more typically on the order of at least 100 years for samples where the age estimates are in closest agreement with the known ages (Barrett 2015; 2017a). For example, with the best sample using the $t^{1/4}$ model the uncertainty associated with the OM/OC ratio leads to an age range for *Joy* of 321-489 years. If the mid-point in the

738 range is used[3] this can be re-written as 405±84 years, or a percentage uncertainty of 20%. For the best samples using
739 $t^{1/n}$, the age range in *Ann* is 59-182 years, or 120±60 years, a percentage uncertainty of 50%. The effects are quite
740 considerable, then, but do not explain the issue of large ages in most samples.

741 It is clear then that the presence of organic matter is a serious issue for RHX dating, as previously stated by Numrich
742 et al. (2015), not alone because of the magnitude in which it can occur, but also because it has been found to be present
743 in significant quantities in all samples (only *Lan* had very low levels), whether the samples were buried during their
744 lifetimes or just exposed to atmospheric conditions. This ubiquitous presence of organic matter raises further questions
745 (in addition to those previously raised by Le Goff and Gallet 2015a; see also the review in Barrett 2015) surrounding
746 good RHX dates obtained in previous studies, where the presence of organic matter was either not examined or treated
747 in a very limited fashion (Wilson et al. 2009; 2012; discussed further in Barrett 2015). It also may be a contributor to
748 poor dates obtained in other studies where the organic matter was not quantified (for example Burakov and Nachasova
749 2013; Le Goff and Gallet 2014; 2015a). Therefore, in all future RHX dating trials the presence of organic matter
750 needs to be examined out and, if suitable quantification is not possible, a method of its removal is required. Wet
751 chemistry methods may be an option. Numrich et al. (2015) consider the removal of contamination as mandatory and
752 tested several wet chemistry pre-treatments (acid-base leaching, wet oxidation) for the removal of organic carbon. All
753 approaches reduced the carbon content (oxidation, H_2O_2, proving most successful) but none were successful in
754 providing a complete removal; for this reason the authors recommended pre-treatment cleaning of RHX samples
755 before mass gain tests, with samples still displaying large carbon content following treatment to be discarded. They
756 also stress that these treatments could potentially remove some hydroxyls, or lead to additional hydroxylation. Further
757 work examining the composition (e.g. mineralogy, surface area) and mass loss change in contaminant-free samples
758 with different pre-treatments would be very useful; note that consideration must also be given to the potential effects
759 heating conducted during pre-treatment (Numrich et al. used 60°C for durations of 60-755 minutes) might have on
760 accelerating the rehydroxylation in the ceramics (see the discussion on short term elevated temperature event
761 (STETES) in Barrett 2015).

762

[3] The age estimate based on an OM/OC of 1.95 was 399yrs old. However, the effects of uncertainties on the age are not symmetric, because the age is proportional to mass[4].

4.3 Mineral Alteration

The differences between the reheated and non-reheated XRD and FTIR spectra showed no appreciable differences (see for example *Figure 9*) associated with mineral alteration during reheating at 500°C, samples *Mac* and *Bel* aside. In associated work (Barrett 2015), it is demonstrated (using XRD, FTIR, petrography) that all samples, with the exception of *Etr* and *Rom*, were likely fired at temperature exceeding 850°C, indicated by the presence of high-temperature mineral phases such as cristobalite, spinel and gehlenite. For *Etr* and *Rom* there is some evidence (calcite breakdown) suggesting original firing temperatures exceeding 650°C. Therefore, the results generally apply to well fired samples but are also the case for moderately fired samples. Given the reasonably large set of compositionally diverse samples examined (see Barrett 2015; 2017a; 2017b for details on composition), mass loss associated with mineralogical changes during the reheating stage of RHX is not found to be problematic, aside from gypsum related problems, supporting the findings in Gallet and Le Goff (2015, Figure 1). Also of note is that no mineralogical changes associated with goethite dehydroxylation were observed and, hence, no related mass loss issues (Burakov and Nachosova 2013).

For *Mac* and *Bel*, mineralogical changes, *Figures 10-11*, are associated with the presence and dehydration of hydrated calcium sulfates (gypsum $CaSO{\cdot}2H_2O$, bassanite $CaSO{\cdot}0.5H_2O$) to anhydrite ($CaSO$), that occur typically in the temperature range 120-160°C (Dunham 1992). For *Mac* and *Bel*, the presence of gypsum was also detected in associated work, precipitated in the pores using petrography and also with sulphur detected using p-XRF ((Barrett 2015). The emission of SO_2 at temperatures exceeding 650-700°C, attributable to gypsum decomposition, is also observed in the TG-MS data, *Table 3* and *Figure 11*.

The presence of gypsum and its dehydration during heating at 500°C for samples *Mac* and *Bel* is also associated with a large difference between the *S1* mass gains, m_{S1}, of the 130C and 500C components (25°C aging), for example *Figure 12* and *Table 5*, a difference not found to be significant in the other samples (Barrett 2015). There are then two possible issues associated with gypsum. Firstly, there is a mass of water loss during dehydration of gypsum when the samples are heated between 130-500°C; this mass loss will be included falsely in the total fractional mass estimate, m_{RHXC}, resulting in an erroneous increase in the age estimate. Secondly, if the level of physisorption is reduced following the conversion of gypsum/bassanite to anhydrite, then the magnitude of this difference will also be reflected

as an increase in the total fractional mass estimate (the estimation of the total fractional mass requires that the level of physisorption is the same for both the 130°C and 500°C components).

In the present work, there is no estimate available for the mass loss due to dehydration of gypsum but an estimate for the change in physisorption level is available. This is worth commenting on in terms of the magnitude of the effect it might have on the age estimates in Barrett (2015;2017a), particularly considering that *Mac* has the highest mass discrepancy (0.00513 and 0.00504, fractional mass for $t^{1/4}$ and $t^{1/n}$ models, respectively; the mass discrepancy corresponds to the quantity of excess mass the RHX mass, m_{RHX}, used in age estimates needs to be reduced by to find agreement with the known age) of all samples for both models and *Bel* is the second highest for the $t^{1/n}$ model (0.00079 and 0.00152 for $t^{1/4}$ and $t^{1/n}$ models, respectively). The experimental estimates of m_{S1} are only approximate (Barrett 2015), but the differences between the 130°C (the larger gain) and the 500°C components, $m_{S1\text{-}130} - m_{S1\text{-}500}$, are as follows: for *Mac*, 0.00236 ($t^{1/4}$) and 0.00235 ($t^{1/n}$); for *Bel*, 0.00355 ($t^{1/4}$) and 0.00385 ($t^{1/n}$). The magnitude is clearly of a similar order to that observed for the mass discrepancies of these samples, particularly for the $t^{1/n}$ model, and therefore, gypsum dehydration, even only considering its effects on physisorption, may be a very significant contributor to issues encountered with the estimated ages of these particular samples. More focussed work on the hydration properties of anhydrite and gypsum in fired clays following heating is required. Screening of samples for gypsum, particularly brick as gypsum can be produced by the reaction of sulphuric acid and calcite (in the composition of the brick or through leaching of surrounding mortars) during weathering (Prentice 1990; Pavía and Bolton 2000), is recommended together with increased examination of methods for its removal that do not interfere with the RHX methodology.

5. Conclusion

Research conducted within the framework of a larger study examining the mass gain behaviour of archaeological ceramics (predominantly bricks) and the application of an RHX dating methodology (component based approach) has revealed new, or provided a better understanding of, mass loss issues that occur during drying or reheating.

In particular, drying of ceramics by conventional (oven) methods requires a prolonged and indefinite period (minimum of months), well beyond that carried out in existing work. Modelling of loose water not removed is a possible solution, however this requires high precision recording of the mass loss curves during drying. Alternatively, if the prolonged drying is due to removal of chemisorbed water, as argued for by the present author, then incomplete drying is not problematic and issues of remaining loose water could potentially be resolved using a component based approach.

The organic matter present in samples is a serious concern for RHX dating and its validation. All samples, regardless of their retrieval context, had significant quantities of carbon present, corresponding to 10-50% of the total mass loss during reheating. This has been attributed to organic matter, most likely humic related substances or coke. On account of large uncertainties in the organic matter to organic carbon ratios (OM/OC), the estimation of the mass of organic matter removed during reheating is problematic; on account of this, the age range estimates of samples are badly affected, often varying from 20-50% of the age of well-behaved samples in associated dating trials. In future dating trials, screening and alternative methods for estimating the organic matter mass are required.

Mineralogical changes during reheating were generally negligible and not considered problematic with the exception of samples where gypsum is present. Dehydration of gypsum during heating leads to an unwanted component of mass loss that is difficult to quantify. As well as this physisorption levels (*Stage 1*) are altered, requiring some alterations of the equations used in age estimations. Screening of samples is recommended in future work.

The above mass loss issues all have the potential to adversely affect any future RHX dating trials and will require focussed treatment in future work.

Acknowledgments

This work was conducted as Ph.D. research (accessible) made possible through the aid of a Department for Employment and Learning (DEL) Ph.D. studentship for which I am grateful. Acknowledgements are also made of the assistance provided by the School of Geography, Archaeology and Palaeoecology where this research was conducted. I wish to thank the following persons both for aiding source and for providing samples: Prof. Caroline Malone (QUB), Mr. Michael Barrett (Turlough), Dr. Joanne Curran (Consarc Design Group), Mr. Peter Francis (Ballynahinch), Ms. Audrey Gahan (Gahan and Long Arch. Serv. Ltd), Mr. Stephen Gilmore (Northern Arch. Cons. Ltd), Mr. Barrie Hartwell (GAP, QUB), Mr. Paul Logue (N. Ireland Environment Agency), Dr. Sara Pavía (Trinity College Dublin), Mr. Cormac McSparron and Mr. Ruairí Ó Baoill (Centre for Archaeological Fieldwork, QUB). For technical assistance and advice, I thank the following persons: Mr. Pat McBride (QUB), Mr. John Meneely (QUB), Mr. Peter Gray, Mr. Stephen Roper, and Mr. Jim McDonald (^{14}CHRONO Centre, QUB), Dr. Jennifer McKinley (GAP, QUB), Dr. John Caulfield (SPACE, QUB), Dr. Rory Flood (GAP, QUB), Mr. Mark Russell (SPACE, QUB) Mr. William Harra (ASEP, QUB).

I also wish to thank Prof. Paula Reimer for her helpful comments with regard to preparation of this text.

863 **References**

864 Barrett, G. T. 2015. *Rehydroxylation Dating: Assessment for Archaeological Application.* School of Geography,
865 Archaeology and Palaeoecology, Queen's University Belfast. Unpublished Ph.D. thesis.
866 http://pure.qub.ac.uk/portal/en/publications/rehydroxylation-dating-assessment-for-archaeological-
867 application(9c89d2bd-ceaf-4f3d-a9d0-515eb23e6204).html (accessed 19/01/17)

868 Barrett, G. T. 2017a. Rehydroxylation (RHX) dating: Trials on post-medieval brick using a component based
869 approach. *Journal of Archaeological Science: Reports.* (accepted)

870 Barrett, G. T. 2017b. Processes and kinetics of mass gain in archaeological brick following drying and reheating.
871 *Journal of American Ceramic Society.* (accepted)

872 Benedetto, G. E. de, Laviano, R., Sabbatini, L. and Zambonin, P. G. 2002. Infrared spectroscopy in the
873 mineralogical characterization of ancient pottery. *Journal of Cultural Heritage*. **3** 177-186

874 Bowen, P. K., Ranck, H. J., Scarlett, T. J. and Drelich, J. W. 2011. Rehydration / rehydroxylation kinetics of
875 reheated XIX-century Davenport (Utah) Ceramic. *Journal of the American Ceramic Society.* **94** 2585-2591

876 Bowen, P. K., Drelich, J. and Scarlett, T. J. 2013. Modeling rehydration/rehydroxylation mass-gain curves from
877 Davenport ceramics. *Journal of the American Ceramic Society.* **96** 885-891

878 Brosnan, D. A. and Robinson, G. C. 2003. *Introduction to Drying of Ceramics*. The American Ceramic Society. p.
879 69

880 Brunswick, R. W. 1990. *Brick Building in Britain.* Victor Gollancz Ltd. London.

881 Burakov, K. S. and Nachasova, I. E. 2013. Archaeomagnetic study and rehydroxylation dating of fired-clay ceramics.
882 *Izvestiya, Physics of the Solid Earth.* **49** 105-112

883 Chen, Y., Mastalerz, M. and Schimmelmann, A. 2012. Characterization of chemical functional groups in macerals
884 across different coal ranks via micro-FTIR spectroscopy. *International Journal of Coal Geology*. **104** 22-33

885 Chukanov, N. V. 2014. *Infrared Spectra of Mineral Species – Extended Library*. Springer. London.

886 Dunham, A. C. 1992. Developments in industrial mineralogy: I. The mineralogy of brick-making. *Proceedings of the*
887 *Yorkshire Geological Society*. **49** 95-104

888 El-Zanan, H. S., Zielinska, B., Mazzoleni, L. R. and Hansen, D. A. 2009. Analytical determination of the aerosol
889 organic mass-to-organic carbon ratio. *Journal of Air Waste Management Association.* **59** 58-69

890 Fernandes, A. N., Giovanela, M., Esteves, V. I., and de Souza Sierra, M. M. 2010. Elemental and spectral properties
891 of peat and soil samples and their respective humic substances. *Journal of Molecular Structure*. **971** 33-38

892 Ford, W. G. 1967. *The Effect of Heat on Ceramics.* MacLaren and Sons Ltd. London.

893 Gallet, Y and Le Goff, M. 2015. Rehydration and rehydroxylation in ancient ceramics: new constraints from mass
894 gain analyses versus annealing temperatures. *Journal of the American Ceramic Society*. **98** 2738-2744

895 Guisnet, M. and Magnoux, P. 2001. Organic chemistry of coke formation. *Applied Catalysis A: General.* **212** 83-
896 96

897 Hammond, M. 1981. *Bricks and Brickmaking.* Shire Publications Ltd. Oxford.

898 Highscore. 2015. PANalytical X-ray diffraction software website. [Online] *http://www.panalytical.com/Xray-*
899 *diffraction-software/HighScore-with-Plus-option.htm.* [accessed 10th June 2015].

900 ICDD. 2015. International Centre for Diffraction Data PDF-2 Database Website. [Online]
901 *http://www.icdd.com/products/pdf2.htm.* [accessed 10th June 2016].

902 Klingenfuß, C., Roßkopf, N., Walter, J., Heller, C. and Zeitz, J. 2014. Soil organic matter to soil organic carbon ratios
903 of peatland soil substrates. *Geoderma.* **235-236** 410-417

904 Larkin, P. 2011. *Infrared and Raman Spectroscopy; Principles and Spectral Interpretation.* Elsevier. MA.

905 Le Goff, M. and Gallet, Y. 2014. Evaluation of the rehydroxylation dating method: insights from a new measurement
906 device. *Quaternary Geochronology*. **20** 89-98

907 Le Goff, M. and Gallet, Y. 2015a. Evidence for complexities in the RHX dating method. *Archaeometry*. **57** (5) 897-
908 910, doi: 10.1111/arcm.12137

909 Le Goff, M. and Gallet, Y. 2015b. Experimental variability in kinetics of moisture expansion and mass gain in
910 ceramics. *Journal of the American Ceramic Society*. **98** 398-401

911 Lewis, W. K. 1921. The rate of drying of solid materials. *Indus. Eng. Chem. – Sympos. Drying.* **3 (5)** 42

912 Madari, B. E., Reeves III, J. B. Machado, P. L. O. A., Guimarães, C. M., Torres, E. and McCarty, G. W. 2006. Mid-
913 and near-infrared spectroscopic assessment of soil compositional parameters and structural indices in two Ferrasols.
914 *Geoderma*. **136** 245-259

915 Marinos-Kouris, D. and Maroulis, Z. B. 2006. Basic process calculations and simulations in drying. In Mujumbar, A.
916 S. (Ed.) *Handbook of Industrial Drying (3rd Edition)*. CRC Press. Florida. p. 81

917 Moore, D. M. and Reynolds, Jr., R. C. 1997. *X-Ray Diffraction and the Identification and Analysis of Clay Minerals.*
918 2nd Edition. Oxford University Press. Oxford.

919 Numrich, M., Kutschera, W., Steier, P., Sterba, J.H. and Golser, R. 2015. On the effect of organic carbon on
920 rehydroxylation (RHX) dating. *Journal of Archaeological Science.* doi: 10.1016/j.jas.2015.01.016.

921 Padowski, Z. and Mujumbar, A. S. 2006. Basic process calculations and simulations in drying. In Mujumbar, A. S.
922 (Ed.) *Handbook of Industrial Drying (3rd Edition)*. CRC Press. Florida. p. 53

923 Pavía, S. and Bolton, J. 2000. *Stone, Brick and Mortar: Historical Use, Decay and Conservation of Building Materials*
924 *in Ireland.* Wordwell. Bray.

925 Philip, S., Martin, R. V., Pierce, J. R., Jimenez, J. L., Zhang, Q., Canagaratna, M. R., Spracklen, D. V., Nowlan, C.
926 R., Lamsal, L. N., Cooper, M. J., and Krotkov, N. A. 2014. Spatially and seasonally resolved estimate of the ratio of
927 organic matter to organic carbon. *Atmospheric Environment.* **87** 34-40

928 Pribyl, D. W. 2010. A critical review of the conventional SOC to SOM conversion factor. *Geoderma*. **156** 75-83

Reeves III, J. B. 2012. Mid-infrared spectral interpretation of soils: is it practical or accurate? *Geoderma*. **189-190** 508-513

Rice, P. M. 1987. *Pottery Analysis: a Sourcebook.* University of Chicago Press. Chicago.

Russell, J. D. and Fraser, A. R. 1994. Infrared methods. In Wilson, M. J. (ed.) 1994. *Clay Mineralogy: Spectroscopic and Chemical Determinative Methods.* Chapman and Hall. London. p. 11-67

Ruthenburg, T. C., Perlin, P. C., Liu, V., McDade, C. E. and Dillner, A. M. 2014. Determination of organic matter and organic matter to organic carbon ratios by infrared spectroscopy with application to selected sites in the improved network. *Atmospheric Environment.* **86** 47-57

Tian, D., Liu, X. and Ding, M. 2010. CS_2 extraction and FTIR & GC/MS analysis of a Chinese brown coal. *Mining Science and Technology*. **20** 0562-2565

Turpin, B. J. and Lim, H. J. 2001. Species contributions to PM2.5 mass concentrations: revisiting common assumptions for estimating organic mass. *Aerosol Science and Technology.* **35** 602-610

Van der Marel, H. W. and Beutelspacher, H. 1976. *Atlas of Infrared Spectroscopy of Clay Minerals and their Admixtures. Elsevier*. Amsterdam.

Vergnoux, A., Guilano, M., Di Rocco, R., Domiezel, M., Théraulaz, F. and Doumenq, P. 2011. Quanitative and mid-infrared changes of humic substances from burned soils. *Environmental Research.* **111** 205-214

Wilson, M. A., Carter, M. A., Hall, C., Hoff, W. D., Ince, C., Savage, S. D., McKay, B. and Betts, I. M. 2009. Dating fired-clay ceramics using long-term power law rehydroxylation kinetics. *Proceedings of the Royal Society A.* **465** 2407-2415

Wilson, M. A., Hamilton, A., Ince, C., Carter, M. A. and Hall, C. 2012. Rehydroxylation (RHX) dating of archaeological pottery. *Proceedings of the Royal Society A.* **468** 3476-3493

Worrall, W. E. 1956. The organic matter in clays. *Transactions of the British Ceramic Society.* **55** 689-705

Zhao, S., Bowen, P. K., Drelich, J. W. and Scarlett, T. J. 2015. Reproducibility in rehydroxylation of ceramic artifacts. *Journal of the American Ceramic Society.* **98** 3367-3372